Elemental abundance trends in the Galactic thin and thick disks as traced by nearby F and G dwarf stars

Bensby, Thomas; Feltzing, Sofia; Lundström, Ingemar

Published in:
Astronomy & Astrophysics

DOI:
10.1051/0004-6361:20031213

2003

A&A 410, 527–551 (2003)
DOI: 10.1051/0004-6361:20031213

Astronomy & Astrophysics

Elemental abundance trends in the Galactic thin and thick disks as traced by nearby F and G dwarf stars⋆,⋆⋆

T. Bensby, S. Feltzing, and I. Lundström

Lund Observatory, Box 43, 221 00 Lund, Sweden

Received 14 April 2003 / Accepted 5 August 2003

Abstract. Based on spectra from F and G dwarf stars, we present elemental abundance trends in the Galactic thin and thick disks in the metallicity regime $-0.8 \lesssim$ [Fe/H] $\lesssim +0.4$. Our findings can be summarized as follows. 1) Both the thin and the thick disks show smooth and distinct abundance trends that, at sub-solar metallicities, are clearly separated. 2) For the α-elements the thick disk shows signatures of chemical enrichment from SNe type Ia. 3) The age of the thick disk sample is in the mean older than the thin disk sample. 4) Kinematically, there exist thick disk stars with super-solar metallicities. Based on these findings, together with other constraints from the literature, we discuss different formation scenarios for the thick disk. We suggest that the currently most likely formation scenario is a violent merger event or a close encounter with a companion galaxy. Based on kinematics the stellar sample was selected to contain stars with high probabilities of belonging either to the thin or to the thick Galactic disk. The total number of stars are 66 of which 21 belong to the thick disk and 45 to the thin disk. The analysis is based on high-resolution spectra with high signal-to-noise ($R \sim 48\,000$ and $S/N \gtrsim 150$, respectively) recorded with the FEROS spectrograph on La Silla, Chile. Abundances have been determined for four α-elements (Mg, Si, Ca, and Ti), for four even-nuclei iron peak elements (Cr, Fe, Ni, and Zn), and for the light elements Na and Al, from equivalent width measurements of ∼30 000 spectral lines. An extensive investigation of the atomic parameters, $\log gf$-values in particular, have been performed in order to achieve abundances that are trustworthy. Noteworthy is that we find for Ti good agreement between the abundances from Ti I and Ti II. Our solar Ti abundances are in concordance with the standard *meteoritic* Ti abundance.

Key words. stars: fundamental parameters – stars: abundances – Galaxy: disk – Galaxy: formation – Galaxy: abundances – Galaxy: kinematics and dynamics

1. Introduction

Ever since it was revealed that the Galactic disk contains two distinct stellar populations with different kinematic properties and different mean metallicities their origin and nature have been discussed. The first evidence for the second disk population was offered by Gilmore & Reid (1983) who discovered that the stellar number density distribution as a function of distance from the Galactic plane was not well fitted by a single density profile. A better match was found by using two components with scale heights of 300 pc and 1350 pc, respectively. The latter component was identified as a Galactic *thick disk*, as a complement to the more well-known *thin disk*.

Thick disk stars move in Galactic orbits with a scale height of 800 pc (e.g. Reylé & Robin 2001) to 1300 pc (e.g. Chen 1997), whereas the thin disk stars have a scale height of 100–300 pc (e.g. Gilmore & Reid 1983; Robin et al. 1996). The velocity dispersions are also larger in the thick disk than in the thin disk. Soubiran et al. (2003), for example, find $(\sigma_U, \sigma_V, \sigma_W) = (63 \pm 6, 39 \pm 4, 39 \pm 4)$ km s^{-1}, and $(\sigma_U, \sigma_V, \sigma_W) = (39 \pm 2, 20 \pm 2, 20 \pm 1)$ km s^{-1} for the thick and thin disks, respectively. Further, the thick disk is as a whole a more slowly rotating stellar system than the thin disk. It lags behind the local standard of rest (LSR) by approximately 50 km s^{-1} (e.g. Soubiran et al. 2003). The thick disk is also known to mainly contain stars with ages greater than ∼8 Gyr, e.g. Fuhrmann (1998), while the thin disk is populated by younger stars. The normalization of the densities of the stellar populations in the solar neighbourhood gives a thick disk fraction of 2–15%, with the lowest values from Gilmore & Reid (1983) and Chen (1997), and the highest from Chen et al. (2001) and Soubiran et al. (2003). Robin et al. (1996) and Buser et al. (1999) found values around 6%. A high value of the normalization is usually associated with a low value of the scale height.

The presence of a thick disk in the Milky Way galaxy is not unique. Extra-galactic evidence of thick disks in edge-on galaxies is continuously growing (e.g. Reshetnikov & Combes 1997; Schwarzkopf & Dettmar 2000; Dalcanton & Bernstein 2002).

Send offprint requests to: T. Bensby, e-mail: thomas@astro.lu.se

⋆ Based on observations collected at the European Southern Observatory, La Silla, Chile, Proposals #65.L-0019(B) and 67.B-0108(B).

⋆⋆ Full Tables 3 and 6 are only available in electronic form at the CDS via anonymous ftp to
cdsarc.u-strasbg.fr (130.79.128.5) or via
http://cdsweb.u-strasbg.fr/cgi-bin/qcat?J/A+A/410/527

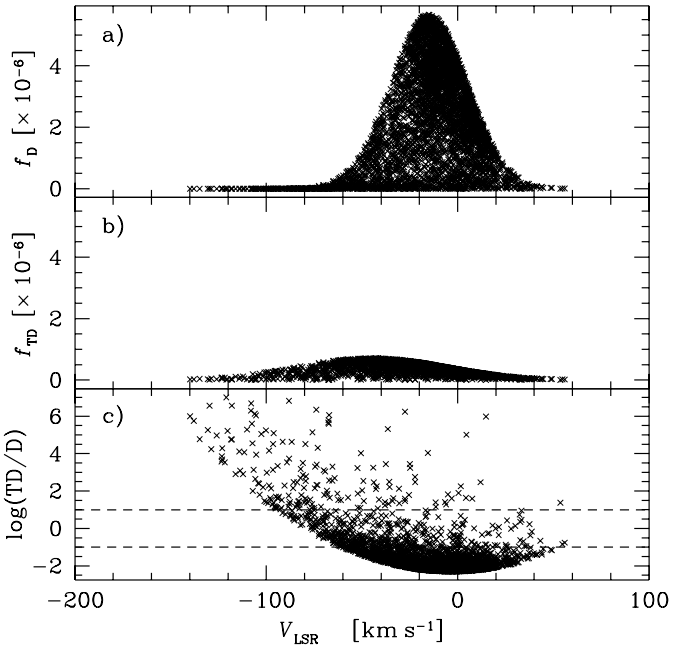

Fig. 1. a) and **b)** show the f_D and the f_{TD} "probabilities", Eq. (1), and **c)** the TD/D relative probabilities, Eq. (3). Dashed lines indicate TD/D = 10 and TD/D = 0.1.

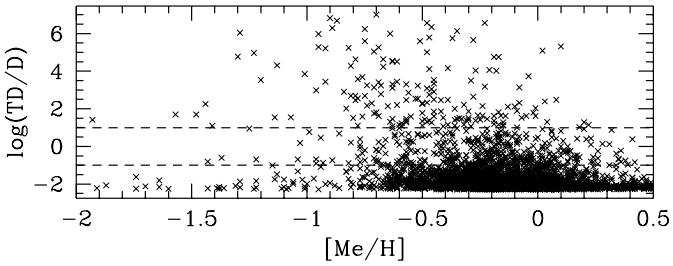

Fig. 2. The TD/D "relative probabilities" versus photometric metallicity for the whole catalogue. Dashed lines indicate TD/D = 10 and TD/D = 0.1.

There are essentially two major formation scenarios for the Milky Way thick disk. First, we have the *merger scenario* in which the thick disk got puffed up as a result of a merging event with a companion galaxy (e.g. Robin et al. 1996) and as a consequence star formation stopped ∼8 Gyrs ago. However, Kroupa (2002) shows that the Milky Way actually does not have to merge with another galaxy to produce a kinematical heating of the galactic disk. An episode of kinematical heating and increased star formation can be caused by a passing satellite. Second, we have the possibility that the thin and thick disk form an *evolutionary sequence*. In this scenario the thick disk formed first and once star formation had stopped the remaining gas (maybe replenished through in-fall) settled in to a thin disk with a smaller scale height. The initial collapse can be either a slow, pressure supported collapse or a fast collapse due to increased dissipation (e.g. Burkert et al. 1992). The main difference between these two is that vertical abundance gradients will have time to build up in the thick disk in the slow collapse, while results from modelling indicate that there is not enough time to build up such gradients in a fast collapse. In the model by Burkert et al. (1992) star formation in the thick disk ceases after only ∼400 Myr. Naively, both the merging and the collapse scenarios predict that the lowest age for a thick disk star must be greater than the highest age for a thin disk star. It also appears plausible in both scenarios that the mean metallicity of the thin disk should be higher than that of the thick disk. But, because in-fall is most likely needed in order to produce the stars in the thin disk the actual *distributions* of metallicities in the two components should be overlapping.

In addition to the two major scenarios discussed above several other ways of producing the kinematical and density distributions found in the two disks have been proposed (see e.g. Gilmore et al. 1989). Noteworthy is the *direct accretion of material* scenario in which extra-galactic debris ends up in the Milky Way and finally forms a larger entity, the thick disk. This scenario will most likely result in a stellar population with a wide spread in age and metallicity. Another possibility is that the thick disk formed as a result of *kinematic diffusion of stellar orbits*, i.e. stars in a thin disk are influenced by their surroundings and their orbits will change with time due to interaction with e.g. giant molecular clouds or "collisions" with other stars. In this formation scenario for the thick disk the stars of the thin and the thick disks have the same origin. Also note that, in this case, the formation time for the thick disk must be long as diffusion of orbits is a slow process.

Recently, the chemical evolution of the stellar population in the thick disk has become a subject of intense study and discussion (e.g. Mashonkina & Gehren 2001; Tautvaišienė et al. 2001; Chen et al. 2000; Gratton et al. 2000; Prochaska et al. 2000; Fuhrmann 1998). The evidence from these studies points in conflicting directions. While Gratton et al. (2000) conclude that the time scale for the formation of the thick disk is less than 1 Gyr, Prochaska et al. (2000) infer a time scale longer than 1 Gyr. The estimate by Mashonkina & Gehren (2001) falls in between these two estimates and they also found that the gas out of which the thick disk formed had been enriched by s-process nuclei. Further Chen et al. (2000) found that the chemical trends of the thin disk follow smoothly upon those of the thick disk, while Fuhrmann (1998) and Prochaska et al. (2000) both found the chemical trends in the thin and the thick disks to be disjunct. None of these studies include thick disk stars with metallicities higher than [Fe/H] ∼ −0.3.

In this paper we will investigate the elemental abundance trends of two kinematically distinct stellar samples that can be associated with the thin and the thick Galactic disks, respectively. We will not use criteria on stellar ages and metallicities when we select our samples. This means that we will probe the thick disk at higher metallicities than what has been done in previous studies. We will show that the stellar populations of the thin and the thick disks have distinct and different chemical trends. This is most likely due to the different origins of the two disks and will be further discussed in the paper.

The paper is organized as follows. In Sect. 2 the criteria for the selection of stars are described. The observations and data reductions are presented in Sect. 3 and in Sect. 4 we derive new radial velocities for the stars. The determination of the fundamental stellar parameters, as well as elemental abundances, is

Table 1. Characteristic velocity dispersions (σ_U, σ_V, and σ_W) in the thin disk, thick disk, and stellar halo, used in Eq. (1). X is the observed fraction of stars for the populations in the solar neighbourhood and $V_{\rm asym}$ is the asymmetric drift. The values fall within the intervals that are characteristic for the thin and thick disks, see Sect. 1.

	X	σ_U	σ_V	σ_W	$V_{\rm asym}$
		[km s^{-1}]			
Thin disk (D)	0.94	35	20	16	−15
Thick disk (TD)	0.06	67	38	35	−46
Halo (H)	0.0015	160	90	90	−220

described in Sect. 5. In Sect. 6 we describe the atomic data, the $\log gf$-values in particular, that have been used in the abundance determination. Section 7 explores the errors, both random and systematic, that are present in the abundance determination, and the most probable error sources. The determination of stellar ages is described in Sect. 8, and then, in Sect. 9, we present our resulting abundances relative to Fe and Mg in terms of diagrams where $[X/Y]$[1] is plotted versus $[Y/{\rm H}]$ (where Y is either Fe or Mg). In Sect. 10 our abundance results are further discussed in the context of Galactic chemical evolution. Constraints are set on the different formation scenarios for the thick disk and we discuss the most likely scenario. Section 11 summarizes our findings.

2. The stellar sample

There is no obvious predetermined way to define a sample of purely thick disk stars (or thin disk stars!) in the solar neighbourhood. There are essentially two ways of finding local thick or thin disk stars; the pure kinematical approach (that we adopted), or by looking at a combination of kinematics, metallicities, and stellar ages (e.g. Fuhrmann 1998). Both methods will produce, for example, thick disk samples that are "contaminated" with thin disk stars. In this study we have tried to minimize this type of contamination by selecting thin and thick disk stars that kinematically are "extreme members" of their respective population.

The selection of thick and thin disk stars is done by assuming that the Galactic space velocities ($U_{\rm LSR}$, $V_{\rm LSR}$, and $W_{\rm LSR}$, see Appendix A) of the stellar populations in the thin disk, the thick disk, and the halo have Gaussian distributions,

$$f(U,\,V,\,W) = k \cdot \exp\left(-\frac{U_{\rm LSR}^2}{2\,\sigma_U^2} - \frac{(V_{\rm LSR} - V_{\rm asym})^2}{2\,\sigma_V^2} - \frac{W_{\rm LSR}^2}{2\,\sigma_W^2}\right), \quad (1)$$

where

$$k = \frac{1}{(2\pi)^{3/2}\,\sigma_U\sigma_V\sigma_W} \quad (2)$$

normalizes the expression, σ_U, σ_V, and σ_W are the characteristic velocity dispersions, and $V_{\rm asym}$ is the asymmetric drift. Table 1 lists the values we adopted for the three populations (J. Holmberg 2000, private comm.).

[1] Abundances expressed within brackets are as usual relative to solar values where, for element X, $[X/{\rm H}] = \log(N_X/N_{\rm H})_\star - \log(N_X/N_{\rm H})_\odot$.

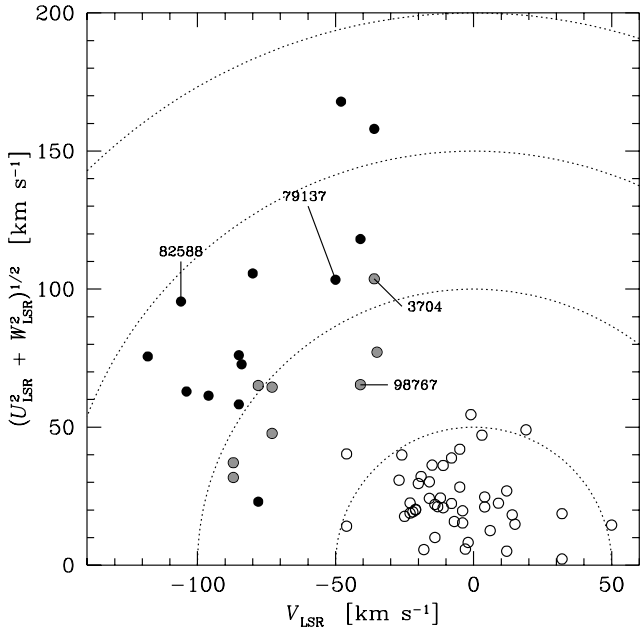

Fig. 3. Toomre diagram for our stellar sample. Dotted lines indicate constant peculiar space velocities, $v_{\rm pec} = (U_{\rm LSR}^2 + V_{\rm LSR}^2 + W_{\rm LSR}^2)^{1/2}$, in steps of 50 km s^{-1}. Stars that we discuss in Sect. 9.4 have been identified with their Hipparcos numbers. Thin disk stars are marked by empty circles and thick disk stars by filled (black: TD/D > 10, grey: 1 < TD/D < 10) circles.

For a given star, when computing the relative likelihoods of belonging to either the thick or the thin disk, one has to take in to account that the local number densities of thick and thin disk stars are different. In the solar neighbourhood 94% of stars belong to the thin disk whereas only 6% belong to the thick disk (according to Robin et al. 1996 or Buser et al. 1999). To really get the probability (which we will call D, TD, and H, for the thin disk, thick disk, and stellar halo, respectively) that a given star belongs to a specific population we therefore have to multiply the probabilities from Eq. (1) by the observed fractions (X) of each population in the solar neighbourhood. By then dividing the thick disk probability (TD) with the thin disk (D) and halo (H) probabilities, respectively, we get two relative probabilities for the thick-disk-to-thin-disk (TD/D) and thick-disk-to-halo (TD/H) membership, i.e.

$$\frac{\rm TD}{\rm D} = \frac{X_{\rm TD}}{X_{\rm D}} \cdot \frac{f_{\rm TD}}{f_{\rm D}}, \qquad \frac{\rm TD}{\rm H} = \frac{X_{\rm TD}}{X_{\rm H}} \cdot \frac{f_{\rm TD}}{f_{\rm H}}. \quad (3)$$

For 10 166 stars (binaries excluded) in the solar neighbourhood, Feltzing et al. (2001) derived photometric metallicities[2] (note that they could only derive good ages for ∼6000 of these stars). As a basis for their determinations they used the Hipparcos catalogue (ESA 1997) and Strömgren photometry from Hauck & Mermilliod (1998). Magnitudes and colours were corrected for interstellar reddening by the model by Hakkila et al. (1997) and for Lutz-Kelker bias by the mean bias correction term from Koen (1992). Effective temperatures were derived using the calibration by Alonso et al. (1996) and

[2] Metallicities derived from photometry are denoted by "[Me/H]". Spectroscopic "metallicities" are denoted by "[Fe/H]" and measure the iron content of the stars.

Table 2. Stellar parameters for our program stars. The first three columns give the identification of each star, Hipparcos, HD, and HR numbers. The fourth column gives the spectral class as listed in Simbad. The fifth to the seventh columns give V, π, and σ_π, all from the Hipparcos catalogue. Columns 8 to 10 give the fundamental parameters, metallicity, effective temperature, and surface gravity that we derive and Col. 11 the microturbulence (see Sect. 5). Column 12 gives the masses that we derive and Col. 13 the bolometric corrections used in Sect. 5.2.3. Columns 14 to 17 list the radial velocities measured by us and the subsequently calculated U, V, and W velocities relative to the local standard of rest (LSR). Columns 18 and 19 give the relative probabilities of the thick disk-to-thin disk and thick disk-to-halo memberships, respectively. The last three columns (20 to 22) give the results of our age determinations, see Sect. 8. In the last column an "s" indicates that Salasnich et al. (2000) isochrones were used when determining the stellar age, a "g" that Girardi et al. (2000) isochrones were used, and an "sg" that the combination of both sets of isochrones were used.

Identifications			Sp. type	V	π	σ_π	[Fe/H]	$T_{\rm eff}$	$\log g$	$\xi_{\rm t}$	$\mathcal{M}$	BC	$v_{\rm r}$	$U_{\rm LSR}$	$V_{\rm LSR}$	$W_{\rm LSR}$	TD/D	TD/H	Age	Min/max	
Hip	HD	HR		[mag]	[mas]	[mas]		[K]	[cgs]	[km s^{-1}]	[$M_\odot$]	[mag]	[km s^{-1}]						[Gyr]	[Gyr]	
THIN DISK STARS																					
3142	3735	170	F8V	6.68	24.12	0.82	−0.45	6100	4.07	1.50	1.12	−0.12	−13.2	−35	−46	20	0.06	>999	5.6	5.1 / 6.3	s
7276	9562	448	G2IV	5.75	33.71	0.72	0.20	5930	3.99	1.35	1.22	−0.09	−13.3	1	−21	20	0.01	>999	3.2	2.7 / 4.5	g
9085	12042	573	F6.5V	6.10	37.97	0.61	−0.31	6200	4.25	1.30	1.06	−0.10	5.7	−42	−5	1	0.01	>999	5.9	5.0 / 8.0	g
10798	14412	683	G5V	6.33	78.88	0.72	−0.47	5350	4.57	0.20	0.84	−0.23	6.2	−1	32	−2	0.01	>999	–	– / –	
12186	16417	772	G5IV	5.78	39.16	0.64	0.14	5800	4.04	1.20	1.10	−0.11	13.0	32	−19	−3	0.01	>999	5.8	3.8 / 6.3	g
12611	17006	807	K1III	6.09	24.47	0.56	0.26	5250	3.66	1.35	1.46	−0.24	14.4	22	−14	0	0.01	>999	2.8	2.6 / 3.0	g
12653	17051	810	G0V	5.40	58.00	0.55	0.14	6150	4.37	1.25	1.15	−0.07	18.5	−21	−13	−3	0.01	>999	–	– / –	
14954	19994	962	F8V	5.07	44.69	0.75	0.19	6240	4.10	1.60	1.33	−0.06	18.1	−10	−14	1	0.01	>999	2.3	2.0 / 2.6	g
17378	23249	1136	K0IV	3.52	110.58	0.88	0.24	5020	3.73	0.80	1.18	−0.33	−4.0	−5	32	18	0.02	>999	4.5	4.3 / 5.0	g
22263	30495	1532	G3V	5.49	75.10	0.80	0.05	5850	4.50	0.95	1.10	−0.11	23.9	−15	−4	3	0.01	>999	–	– / –	
22325	30606	1538	F8V	5.76	24.06	0.75	0.06	6250	3.91	1.80	1.55	−0.07	36.4	−20	−8	−10	0.01	>999	2.2	2.1 / 2.3	g
23555	32820	1651	F8V	6.30	31.93	0.57	0.13	6300	4.29	1.50	1.23	−0.06	32.8	−23	−12	−8	0.01	>999	2.4	1.2 / 3.3	g
23941	33256	1673	F2V	5.11	39.99	0.70	−0.30	6427	4.04	1.90	1.24	−0.08	12.2	−2	−2	8	0.01	>999	3.5	2.3 / 4.5	g
24829	35072	1767	F7III-IV	5.44	27.70	0.50	0.06	6360	3.93	1.70	1.54	−0.06	46.6	−37	−26	−15	0.01	>999	2.1	2.0 / 2.2	g
29271	43834	2261	G6V	5.08	98.54	0.45	0.10	5550	4.38	0.80	0.90	−0.16	38.2	30	−27	−6	0.01	>999	11.8	6.0 / 16.5	s
30480	45701	2354	G3III-IV	6.45	31.46	0.52	0.19	5890	4.15	1.20	1.09	−0.10	29.4	29	−20	−6	0.01	>999	4.2	3.5 / 6.3	g
30503	45184	2318	G2IV	6.37	45.38	0.63	0.04	5820	4.37	0.90	1.00	−0.12	−1.8	19	9	−12	0.01	>999	6.2	2.2 / 9.6	g
72673	130551		F5V	7.16	20.94	0.88	−0.62	6350	4.18	1.60	1.03	−0.11	32.4	49	−1	24	0.02	>999	6.0	4.7 / 7.2	s
78955	144585	5996	G5V	6.32	34.60	1.00	0.33	5880	4.22	1.12	1.20	−0.09	−14.7	−17	−16	25	0.01	>999	4.6	3.6 / 6.5	g
80337	147513	6094	G5V	5.37	77.69	0.86	0.03	5880	4.49	1.10	1.09	−0.11	13.4	24	4	6	0.01	>999	–	– / –	
80686	147584	6098	F9V	4.90	82.61	0.57	−0.06	6090	4.45	1.01	1.15	−0.09	1.7	18	14	3	0.01	>999	–	– / –	
81520	149612		G3V	7.01	46.13	0.91	−0.48	5680	4.53	0.65	0.90	−0.17	−9.9	−18	−22	7	0.01	>999	5.0	– / 18.0	sg
83601	154417	6349	F8.5IV-V	6.00	49.06	0.89	0.09	6167	4.48	1.21	1.20	−0.07	−16.2	12	−25	−13	0.01	>999	–	– / –	
84551	156098	6409	F6IV	5.53	19.80	0.72	0.12	6475	3.79	2.00	1.85	−0.05	−38.8	−32	−15	17	0.01	>999	1.1	1.0 / 1.2	s
84636	156365		G3V	6.59	21.20	0.92	0.23	5820	3.91	1.30	1.27	−0.11	−12.1	2	4	−21	0.01	>999	3.9	3.7 / 4.2	g
85007	157466		F8V	6.88	33.54	0.84	−0.39	6050	4.37	1.10	0.98	−0.12	33.1	48	19	10	0.01	>999	7.9	4.7 / 10.6	g
85042	157347	6465	G5IV	6.28	51.39	0.85	0.03	5720	4.40	1.00	0.98	−0.13	−35.2	−17	−11	−12	0.01	>999	8.5	4.2 / 12.6	g
86731	161239	6608	G2IIIb	5.73	26.13	0.63	0.25	5840	3.79	1.43	1.40	−0.10	−24.4	−15	−16	19	0.01	>999	2.7	2.3 / 3.2	sg
86796	160691	6585	G3IV-V	5.12	65.46	0.80	0.32	5800	4.30	1.05	1.31	−0.10	−10.4	−5	−3	3	0.01	>999	3.9	3.8 / 4.0	g
87523	162396	6649	F8IV-V	6.19	30.55	0.90	−0.40	6070	4.07	1.36	1.11	−0.12	−18.1	−15	−5	−24	0.01	>999	5.9	5.3 / 6.5	s
90485	169830	6907	F9V	5.90	27.53	0.91	0.12	6339	4.05	1.55	1.35	−0.06	−16.4	−6	6	11	0.01	>999	2.5	2.2 / 2.7	g
91438	172051	6998	G5V	5.85	77.02	0.85	−0.24	5580	4.42	0.55	0.78	−0.17	36.0	47	3	3	0.01	>999	–	– / –	
94645	179949	7291	F8V	6.25	36.97	0.80	0.16	6200	4.35	1.20	1.18	−0.07	−23.0	−15	−7	−5	0.01	>999	–	– / –	
96536	184985	7454	F7V	5.46	32.36	0.74	0.03	6397	4.06	1.65	1.43	−0.06	−14.3	10	−23	16	0.01	>999	2.3	2.1 / 2.5	g
98785	190009	7658	F7V	6.44	17.38	0.76	0.03	6430	3.97	1.90	1.61	−0.06	9.9	23	12	14	0.01	>999	1.9	1.8 / 2.0	g
99240	190248	7665	G7IV	3.55	163.73	0.65	0.37	5585	4.26	0.98	0.98	−0.15	−21.1	−38	−8	−8	0.01	>999	9.5	6.8 / 12.6	g
102264	197214		G5V	6.95	44.57	0.87	−0.22	5570	4.37	0.60	0.77	−0.17	−22.9	−3	−21	20	0.01	>999	–	– / –	
103682	199960	8041	G1V	6.21	37.80	1.01	0.27	5940	4.26	1.25	1.16	−0.09	−16.0	4	−18	4	0.01	>999	4.1	2.8 / 5.6	g
105858	203608	8181	F6V	4.21	108.50	0.59	−0.73	6067	4.27	1.17	0.88	−0.14	−31.0	−4	50	14	0.05	>999	10.5	7.8 / 13.3	s
109378	210277		G0	6.54	46.97	0.79	0.22	5500	4.30	0.78	0.90	−0.17	−22.0	14	−46	2	0.02	>999	10.8	6.7 / 15.0	g
110341	211976	8514	F6V	6.18	31.45	0.83	−0.17	6500	4.29	1.70	1.28	−0.07	7.5	5	12	1	0.01	>999	1.1	– / 2.0	g
113137	216437	8701	G2.5IV	6.04	37.71	0.58	0.22	5800	4.10	1.16	1.10	−0.11	−1.4	14	15	5	0.01	>999	6.1	4.1 / 7.2	g
113357	217014	8729	G2.5IVa	5.45	65.10	0.76	0.20	5789	4.34	1.00	1.07	−0.11	−31.8	−5	−23	22	0.01	>999	4.8	1.8 / 7.4	g
113421	217107	8734	G8IV	6.17	50.71	0.75	0.35	5620	4.29	0.97	0.95	−0.14	−14.3	8	−4	18	0.01	>999	8.3	5.0 / 11.0	g
117880	224022	9046	F8IV	6.03	35.86	0.80	0.12	6100	4.21	1.30	1.21	−0.08	−7.4	−36	−11	3	0.01	>999	4.2	3.3 / 5.7	g

metallicities by the calibration of Schuster & Nissen (1989). For all stars, in Feltzing et al. (2001), with radial velocities from Barbier-Brossat et al. (1994) and positions and proper motions from the Hipparcos catalogue we calculated Galactic velocity components, $U_{\rm LSR}$, $V_{\rm LSR}$ and $W_{\rm LSR}$, relative to the local standard of rest (LSR) (see Appendix A). Since not all stars in Feltzing et al. (2001) have measured radial velocities the final sample, out of which we select our target stars, contains approximately 4500 stars.

In Figs. 1a and b we show the thin and thick disk probability distributions, calculated with Eq. (1), and in Fig. 1c the TD/D distribution, calculated with Eq. (3). In order to try to minimize the contamination of thin disk stars in the thick disk sample we originally selected thick disk stars as those with TD/D ≥ 10, i.e. those stars that are at least ten times more likely to be a thick disk star than a thin disk star. Thin disk stars were consequently selected from those that are at least ten times more likely of being a thin disk star than a thick disk star (TD/D ≤ 0.1). These dividing lines have been marked in Fig. 1c by dashed lines. According to these criteria the full sample contains 180 thick disk stars and ~3800 thin disk stars. Figure 2 also shows the TD/D distribution versus metallicity for the catalogue, ~4500 stars. However, it should be noted that these limits are by no means definite and indeed investigations of HR-diagrams resulting from different cuts indicate that more relaxed criteria are possible. This is especially true for the thick disk.

The stellar samples analyzed in this article originate from two observing proposals (programs) 65.L-0019 (*new constraints on models of galactic chemical evolution from oxygen abundances in dwarf stars with [Me/H] > 0.0*) and 67.B-0108 (*the chemical evolution of the thick disk as seen through oxygen abundances*). Both these programs utilized the FEROS as well as the CES spectrographs. As our observations with the

Table 2. continued.

Identifications			Sp. type	V	π	σ_π	[Fe/H]	$T_{\rm eff}$	$\log g$	$\xi_{\rm t}$	$\mathcal{M}$	BC	$v_{\rm r}$	$U_{\rm LSR}$	$V_{\rm LSR}$	$W_{\rm LSR}$	TD/D	TD/H	Age	Min/max	
Hip	HD	HR		[mag]	[mas]	[mas]		[K]	[cgs]	[km s^{-1}]	[$M_\odot$]	[mag]	[km s^{-1}]						[Gyr]	[Gyr]	
THICK DISK STARS																					
3086	3628		G2V	7.34	21.79	0.88	−0.11	5840	4.15	1.15	1.07	−0.12	−25.5	−159	−48	54	>999	128	6.8	5.6 / 7.5	s
3185	3795	173	G3/G5V	6.14	35.02	0.74	−0.59	5320	3.78	0.70	0.88	−0.24	−44.7	−37	−85	45	76	461	12.1	11.5 / 14.1	s
3497	4308		G5V	6.55	45.76	0.56	−0.33	5636	4.30	0.80	0.85	−0.17	94.1	60	−104	−19	239	269	16.3	12.0 / 20.0	s
3704	4597		F7/F8V	7.85	19.99	0.94	−0.38	6040	4.30	1.08	0.98	−0.12	−36.9	86	−36	58	23.5	705	8.4	6.5 / 11.5	g
5315	6734		K0IV	6.44	21.53	0.83	−0.42	5030	3.46	0.86	1.10	−0.32	−95.8	60	−118	46	>999	62.6	6.2	3.6 / 11.5	s
14086	18907	914	G5IV	5.88	32.94	0.72	−0.59	5110	3.51	0.87	0.81	−0.30	41.9	19	−78	−13	1.2	>999	17.0	10.3 / –	s
17147	22879		F9V	6.68	41.07	0.86	−0.84	5920	4.33	1.20	0.82	−0.16	119.2	−99	−80	−37	170	325	14.0	9.0 / 18.0	s
75181	136352	5699	G4V	5.65	68.70	0.79	−0.34	5650	4.30	0.78	0.85	−0.17	−69.7	−110	−41	43	12.0	719	15.9	11.9 / 19.0	s
79137	145148	6014	K1.5IV	5.93	32.84	0.96	0.30	4900	3.62	0.60	1.30	−0.39	−4.3	82	−50	−63	112	482	3.7	3.3 / 4.7	g
82588	152391		G8V	6.65	59.04	0.87	−0.02	5470	4.55	0.90	0.95	−0.19	44.4	94	−106	17	>999	154	6.0	– / 16.0	g
83229	153075		G1V	6.99	31.77	0.85	−0.57	5770	4.17	0.97	0.79	−0.16	98.5	71	−84	−16	13.0	627	18.3	16.0 / 19.9	s
84905	157089		F9V	6.95	25.88	0.95	−0.57	5830	4.06	1.20	0.91	−0.15	−163.1	−158	−36	−3	22.3	459	11.2	10.4 / 11.9	s
88622	165401		G0V	6.80	41.00	0.88	−0.46	5720	4.35	0.80	0.88	−0.16	−119.9	−69	−85	−32	39.2	492	13.2	8.2 / 17.0	s
96124	183877		G5IV	7.14	38.38	1.09	−0.20	5590	4.37	0.78	0.84	−0.17	−43.6	−28	−87	−15	5.6	817	10.2	4.0 / 15.0	s
98767	190360	7670	G6IV+..	5.73	62.92	0.62	0.25	5490	4.23	0.66	0.90	−0.17	−46.3	−3	−41	−57	2.7	>999	12.0	9.0 / 15.0	g
103458	199288		G0V	6.52	46.26	0.81	−0.65	5780	4.30	0.90	0.77	−0.16	−9.2	31	−96	53	>999	215	19.2	15.0 / –	s
108736	208988		G0V	7.12	27.96	0.86	−0.38	5890	4.24	1.05	0.96	−0.13	−28.0	−16	−73	45	9.6	845	9.9	7.5 / 11.7	s
109450	210483		G1V	7.57	20.58	0.78	−0.13	5830	4.18	1.10	1.05	−0.13	−71.8	−64	−73	−8	1.5	>999	7.2	4.5 / 8.4	s
109821	210918	8477	G5V	6.23	45.19	0.71	−0.08	5800	4.29	1.05	0.99	−0.13	−17.7	−37	−87	−3	4.3	858	7.3	4.6 / 10.0	s
110512	212231		G2V	7.87	18.77	0.89	−0.30	5770	4.15	1.05	0.95	−0.14	7.2	−57	−35	−52	2.3	>999	11.4	10.0 / 11.9	s
118115	224383		G2V	7.89	20.98	1.24	−0.01	5800	4.30	1.00	1.00	−0.12	−29.6	−65	−78	3	2.8	>999	8.7	6.0 / 11.0	g

CES were very time-consuming we had to limit ourselves to stars brighter than $V < 8$ (≈3 hours on the CES). This left 56 stars with TD/D > 10 that were bright enough and that also had suitable metallicities. Of these 29 were observable from La Silla on the observing night with FEROS for the thick disk program. However, the mount of the ESO 1.5 m telescope limits the number of available stars further as did the full Moon. This meant that, in order to sample the full metal range of the thick disk, we had to relax our selection criteria. Hence we have observed 13 thick disk stars with TD/D > 10 and 8 thick disk stars with 1 < TD/D < 10. As we will see in the abundance analysis, see Sect. 9 (and especially Sects. 9.3.2 and 9.4), all but one of the stars in these two groups of thick disk stars trace exactly the same abundance trends. The number of thin disk stars (TD/D < 0.1) is 45. We list all probabilities in Table 2[3]. Figure 3 shows the Toomre diagram for our samples.

3. Observations and data reductions

Observations were carried out with ESO's 1.52 m telescope on La Silla, Chile, on 16th September 2000 (SF and TB as observers) and 28th August 2001 (TB as observer). By using the Fiber Extended Range Optical Spectrograph (FEROS) the complete optical spectrum from 3560 Å to 9200 Å was recorded in one exposure with a resolving power of $R \sim 48\,000$ for each star. We aimed for a signal-to-noise ratio (S/N) of about 250 at 5500 Å, but due to weather conditions the final values are usually around 150. We also obtained integrated solar spectra by observing the late afternoon sky. These spectra have $S/N > 300$.

The FEROS data were reduced using the MIDAS[4] context "feros" which was especially developed for the FEROS data format. The CCD images were processed in the following way: First the different echelle orders are defined from a flat field image. The background consists of several components; the bias level (determined from the over-scan region), dark current (determined from a series of long dark exposures), and scattered light which is smoothly varying over the CCD. The latter is determined from regions outside the spectrum, i.e. between orders and between the two fibers. Dark current is subtracted before scattered light is subtracted. Next the spectral orders are extracted. This is done by an optimum extraction algorithm that also detects and removes cosmic ray events. The flat-fielding is done by dividing the extracted object spectrum with the flat-field spectrum. Wavelength calibration uses ThAr calibration frames and the extracted spectrum is re-binned to constant steps in wavelength. Finally the different orders are merged into a single spectrum.

4. Radial velocities

Since the selection of the stellar sample was based on the $U_{\rm LSR}$, $V_{\rm LSR}$, and $W_{\rm LSR}$ velocities, which were calculated using radial velocities from Barbier-Brossat et al. (1994), we need to confirm the radial velocities in order to verify the calculated probabilities.

We measured line shifts and derived new radial velocities for all 66 stars using Fe I lines with accurate wavelengths from Nave et al. (1994) that were evenly distributed over the whole spectrum. The standard errors of the average radial velocities from these lines are generally below 0.4 km s^{-1}. Agreement with the radial velocities from Barbier-Brossat et al. (1994) is good with only one thick disk star (Hip 14086) having a significantly different value. However, this deviation does not affect the star's initial classification as a thick disk star. The new velocities are given in Table 2.

[3] The actual probabilities listed in Table 2 have been calculated using radial velocities that we determined from our FEROS spectra, see Sect. 4.

[4] ESO-MIDAS is the acronym for the European Southern Observatory Munich Image Data Analysis System which is developed and maintained by the European Southern Observatory.

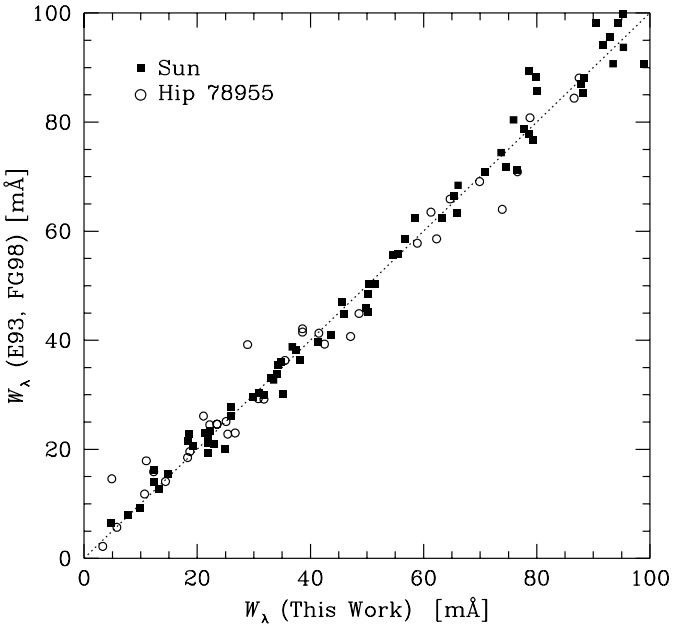

Fig. 4. Equivalent widths measured in the Sun and the metal-rich star Hip 78955. Comparison for the Sun (filled squares) is made to Edvardsson et al. (1993) (E93), while equivalent widths for Hip 78955 (open circles) are compared to those measured in Feltzing & Gustafsson (1998) (FG98). Equivalent widths from this study are plotted on the abscissa.

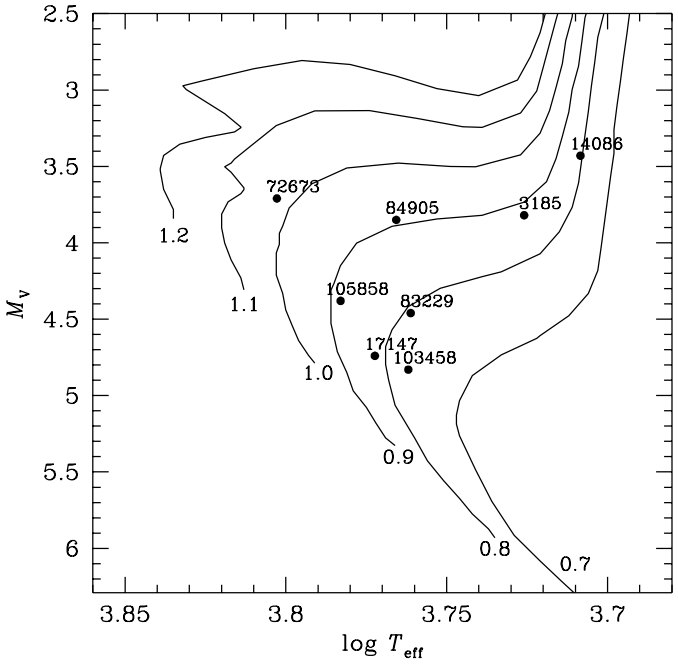

Fig. 5. Example of mass estimates. The evolutionary tracks are from Salasnich et al. (2000) and have a metallicity of −0.74 dex, and the masses they represent are indicated in the figure. The stars shown have [Fe/H] < −0.5 and their Hipparcos numbers have been indicated.

5. Abundance determination

5.1. Equivalent widths

Spectral lines for the analysis were selected using the solar line list by Moore et al. (1966) as well as various sources from the literature (notably Edvardsson et al. 1993; Feltzing & Gustafsson 1998; Stephens 1999; and Nave et al. 1994 for Fe I). The lines were then checked for suitability (line strength, blends, etc.) with guiding help from the solar atlas by Kurucz et al. (1984). The final number of lines is approximately 450, which for our 66 program stars adds up to ∼30 000 equivalent width measurements. The task SPLOT in IRAF[5] was used to interactively measure the equivalent widths (W_λ) of the spectral lines. SPLOT offers several ways of measuring equivalent widths and we chose the option which measures W_λ by fitting a Gaussian, Lorentzian or a Voigt profile to the line. The local continuum was set at every measurement.

In Fig. 4 we compare our equivalent width measurements for the Sun and for one metal-rich star with Edvardsson et al. (1993) and with Feltzing & Gustafsson (1998), respectively. The resolution for the Edvardsson et al. (1993) spectra are $R \sim 80\,000$–$100\,000$ and for the Feltzing & Gustafsson (1998) spectra $R \sim 100\,000$. We have good agreement, although there might be a weak trend for our equivalent widths in the metal-rich stars to be slightly larger than those measured by Feltzing & Gustafsson (1998).

[5] IRAF is distributed by National Optical Astronomy Observatories, operated by the Association of Universities for Research in Astronomy, Inc., under contract with the National Science Foundation, USA.

5.2. Calculation of stellar abundances

Elemental abundances were derived using the Uppsala *Eqwidth* abundance program, maintained by Bengt Edvardsson. As input it needs an opacity table for the stellar atmosphere and a line table with atomic data and the measured equivalent widths.

Opacity tables for the stellar model atmospheres were calculated using the Uppsala MARCS code, originally described by Gustafsson et al. (1975) and Edvardsson et al. (1993) with updated line opacities by Asplund et al. (1997). The models are standard 1-D LTE and require metallicity ([Fe/H]), effective temperature ($T_{\rm eff}$), and surface gravity ($\log g$) as input.

To determine the stellar atmospheric parameters we made use of Fe I lines since they have a wide coverage of line strengths as well as excitation potentials. Fe I (e.g. viz. Fe II) is also by far the most common ion in terms of number of lines in a stellar spectrum.

5.2.1. Effective temperature

Effective temperatures ($T_{\rm eff}$) for the stars were determined by requiring Fe I lines with different lower excitation potentials to produce equal abundances.

5.2.2. Stellar mass

Stellar masses were estimated from the evolutionary tracks by Girardi et al. (2000) and Salasnich et al. (2000) with the same metallicities and α-enhancements as described in Sect. 8. Figure 5 shows an example for stars with [Fe/H] < −0.5, using the α-enhanced tracks from Salasnich et al. (2000) with a metallicity of −0.74 dex.

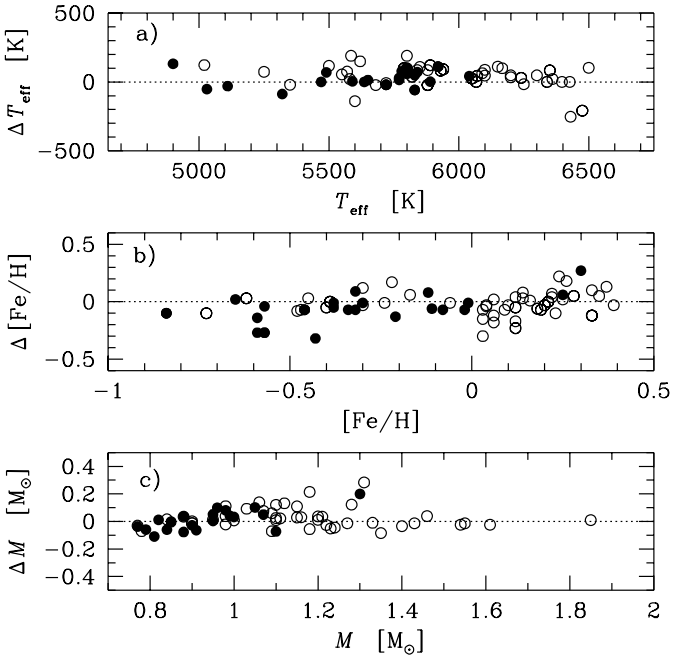

Fig. 6. The difference between our final [Fe/H], $T_{\rm eff}$, and $\mathcal{M}$ and the starting values from Feltzing et al. (2001) as functions of our [Fe/H], $T_{\rm eff}$, and $\mathcal{M}$. Thick and thin disk stars are marked by filled and open circles, respectively.

5.2.3. Surface gravity

A common way to determine $\log g$ is by requiring ionization equilibrium, e.g. that Fe I and Fe II lines produce the same Fe abundance. There are, however, some indications that Fe I is sensitive to departures from LTE while Fe II is not (see e.g. Thévenin & Idiart 1999; Gratton et al. 1999). This could lead to erroneous values for $\log g$.

We therefore instead used the trigonometric parallax and the fundamental relation

$$\log\frac{g}{g_\odot} = \log\frac{\mathcal{M}}{\mathcal{M}_\odot} + 4\log\frac{T_{\rm eff}}{T_{\rm eff\odot}} + 0.4(M_{\rm bol} - M_{\rm bol\odot}), \quad (4)$$

where

$$M_{\rm bol} = V + BC + 5\log\pi + 5. \quad (5)$$

In Eqs. (4) and (5) $\mathcal{M}$ is the stellar mass, $T_{\rm eff}$ is the effective temperature, $M_{\rm bol}$ the absolute bolometric magnitude, V the visual magnitude, BC the bolometric correction, and π the parallax. The stars in our sample are all relatively bright and nearby and therefore have good parallaxes ($\sigma_\pi/\pi < 5\%$, Table 2) determined by the Hipparcos satellite (ESA 1997). Bolometric corrections were interpolated from the grids by Alonso et al. (1995).

5.2.4. Microturbulence

Motions in a stellar atmosphere related to volume sizes that are small compared to the mean free path of a photon are usually referred to as microturbulence ($\xi_{\rm t}$). As long as a spectral line is weak, i.e. not saturated, the microturbulence only makes the line more shallow, conserving its Gaussian shape and equivalent width. However, for stronger lines the total absorption will increase due to a wider wavelength coverage for absorption when the line starts to saturate. Strong lines were therefore rejected. We determined the microturbulence by forcing all Fe I lines to give the same abundance regardless of line strength ($\log W_\lambda/\lambda$).

5.2.5. The final model atmospheres – An iterative process

The fundamental parameters were tuned through the following iterative process:

0. We start by calculating stellar abundances from our equivalent widths using model atmospheres based on $T_{\rm eff}$, $\mathcal{M}$, and [Me/H] from Feltzing et al. (2001). From these abundances diagnostic plots were created and interpreted in the following manner.
1. A slope in the diagram where abundances from individual Fe I lines are plotted versus the lower excitation potential of the lines is interpreted as due to an erroneous temperature. $T_{\rm eff}$ was then altered to get a zero slope. A negative slope requires a decrease of $T_{\rm eff}$ and vice versa for a positive slope. GOTO 2.
2. A slope in the diagram where abundances from individual Fe I lines are plotted versus the line strengths ($\log(W_\lambda/\lambda)$) is interpreted as due to an erroneous microturbulence. $\xi_{\rm t}$ was then altered to get a zero slope. A negative slope requires a lower value for $\xi_{\rm t}$ and vice versa for a positive slope. If $\xi_{\rm t}$ needs to be changed recalculate the abundances with the new $\xi_{\rm t}$ and GOTO 1, else GOTO 3.
3. If the metallicity used when creating the model atmosphere differs from the derived average Fe I abundance change to a new metallicity and calculate a new model atmosphere and new elemental abundances, then GOTO 1, else GOTO 4.
4. Determine the stellar mass. If the new mass differs from the original mass, calculate $\log g$ based on the new mass and create a new model atmosphere and calculate new elemental abundances, then GOTO 1, else GOTO 5.
5. No trends, and consistency between abundances used in the model atmosphere and the calculated abundances. Stellar atmospheric parameters have been tuned.

In this process $\log g$ was automatically altered when changing $T_{\rm eff}$ and/or $\mathcal{M}$ by Eq. (4). Generally less than ten models were generated for each star before the parameters converged. The final values of $T_{\rm eff}$, $\log g$, $\xi_{\rm t}$, and $\mathcal{M}$ are given in Table 2. Figure 6 shows a comparison of our final [Fe/H], $T_{\rm eff}$, and $\mathcal{M}$ to the starting values taken from Feltzing et al. (2001). The average differences are Δ[Fe/H] = -0.02 ± 0.11, $\Delta T_{\rm eff} = +47 \pm 95$ K, and $\Delta\mathcal{M} = +0.02 \pm 0.07\ M_\odot$. This provide an important test of the calibrations used in Feltzing et al. (2001) (see Sect. 2).

As noted in Sect. 5.2.3 there are some indications that Fe I lines are subject to NLTE effects, mainly through overionization in hot stars ($T_{\rm eff} > 6000$ K) with low surface gravities. Since we have not used the Fe II lines (which are supposed to be free from NLTE effects) in the tuning of the stellar

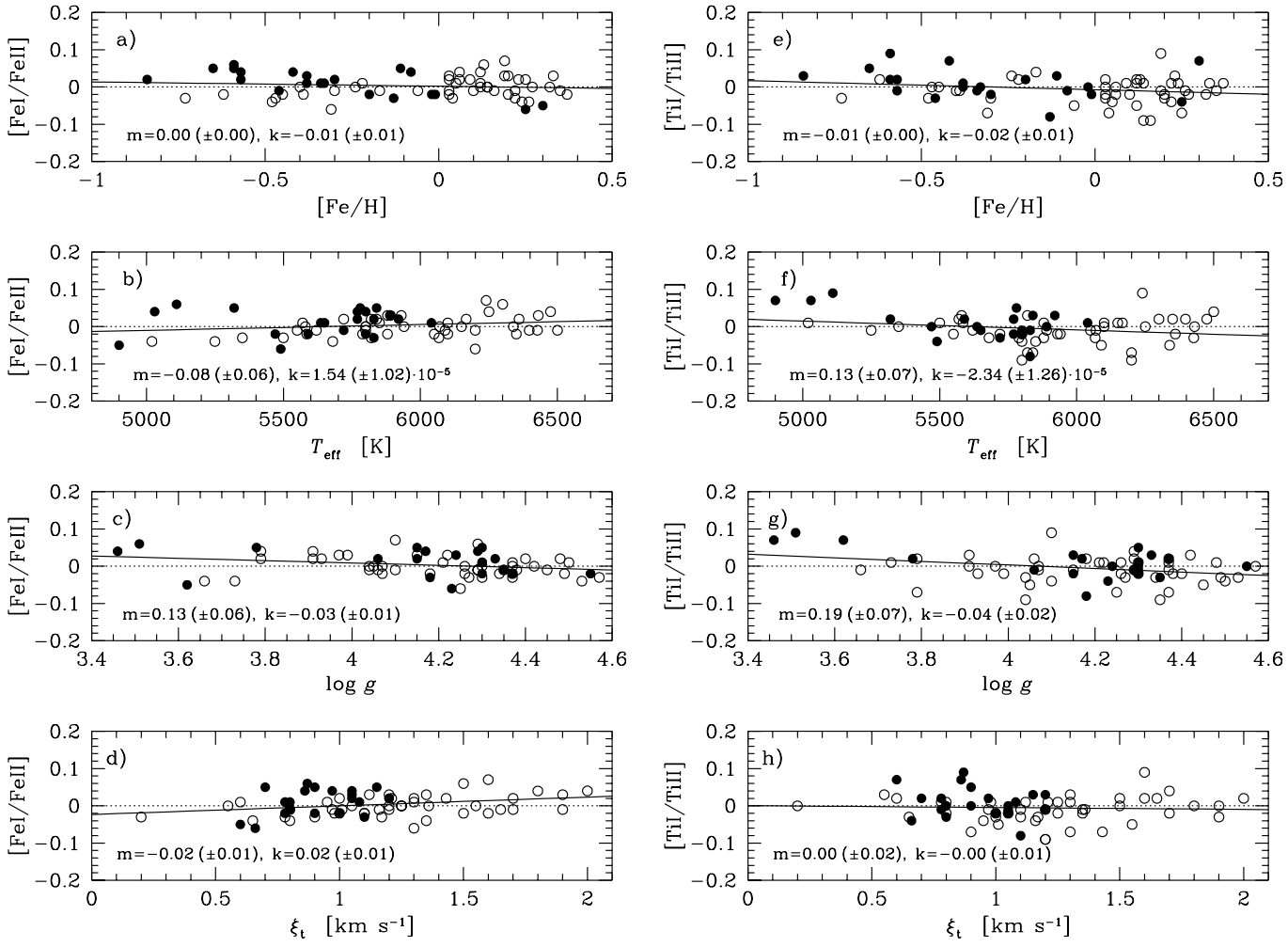

Fig. 7. [Fe I/Fe II] and [Ti I/Ti II] versus [Fe/H], log $T_{\rm eff}$, log g, and $\xi_{\rm t}$. Thin and thick disk stars are marked by open and filled circles, respectively. In each plot we also show, with a solid line, a least square fit and we give the coefficients, slope (k) and constant (m).

atmosphere parameters we utilized them to check on the derived atmospheric parameters as well as the Fe I abundances. In Figs. 7a–d we plot the difference between the derived Fe I and Fe II abundances, [Fe I/Fe II], versus $T_{\rm eff}$, $\xi_{\rm t}$, log g, and [Fe/H] as derived by Fe I lines. We also show the same plots for Ti I and Ti II in Figs. 7e–h. In the plots we also show linear regression lines and their coefficients. As can be seen, the slopes are generally negligible and the offsets at the "zero points" are at the most a few tenths of a dex.

The lack of any discernible trends therefore suggest that Fe I and Ti I do not appear to suffer from appreciable NLTE effects in our sample.

5.3. The solar model atmosphere

For our solar model we used $T_{\rm eff}$ = 5777 K and log g = 4.44 (in cgs units), e.g. Livingston (1999). A consistent value for the microturbulence was harder to find. For example Edvardsson et al. (1993) used $\xi_{\rm t}$ = 1.15 km s^{-1}, Feltzing & Gustafsson (1998) 1.00 km s^{-1}, Chen et al. (2000) 1.44 km s^{-1}, Prochaska et al. (2000) 1.00 km s^{-1}, and Fulbright (2000) 0.80 km s^{-1}. These studies all used reduced equivalent widths to derive the solar microturbulence. Other methods, such as e.g. line profile analysis, usually come out with a lower value of $\xi_{\rm t}$ = 0.5 km s^{-1} (e.g. Gray 1977; Takeda 1995). Our analysis (see Sect. 3), as well as all of the above cited studies, make use of integrated solar light (i.e. the Sun seen as a star).

Figure 8 shows how the Fe I abundance, the spread of the Fe I abundance, and the slope of the solar Fe I abundances from individual lines as a function of reduced equivalent widths (log(W_λ/λ)) vary as functions of $\xi_{\rm t}$. For a correct microturbulence the spread of the derived abundances should reach a minimum and the slope should be zero. As can be seen, the lowest spread in [Fe/H] is for a microturbulence of 0.9 km s^{-1}, Fig. 8a, while the abundance versus line strength shows no trend for a microturbulence of 0.8 km s^{-1} (see Fig. 8b). We therefore adopted a value of 0.85 km s^{-1} for the solar microturbulence. The adherent solar Fe I abundance is ϵ(Fe I)$_\odot$ = 7.56 (see Fig. 8c). The abundance from Fe II for this microturbulence is ϵ(Fe II)$_\odot$ = 7.58, which is in reasonable agreement with the Fe I abundance (see Table 4 and discussion in Appendix B).

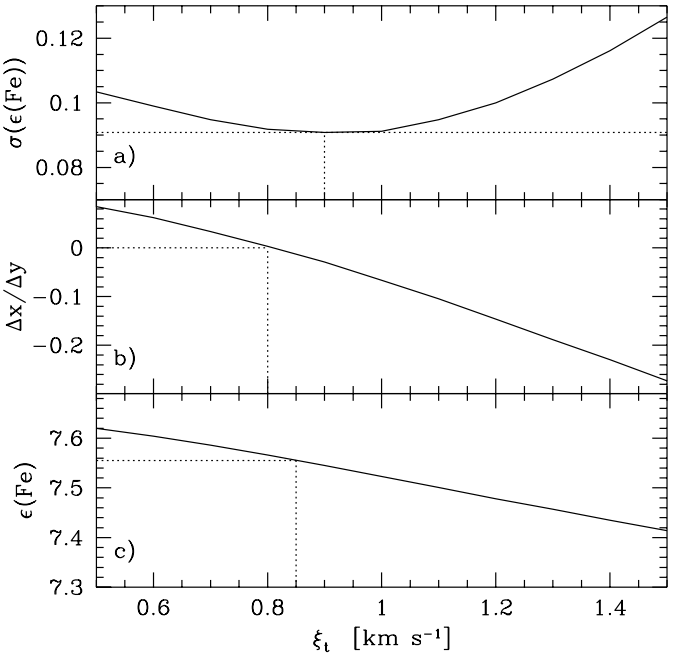

Fig. 8. Determination of ξ_t for the Sun. **a)** The standard deviation of the Fe I abundance. The horizontal dotted line indicates the minimum scatter in [Fe/H] and the vertical line the corresponding ξ_t. **b)** The slope ($\Delta x/\Delta y$) when abundances from individual Fe I lines are plotted versus line strength, $\log(W_\lambda/\lambda)$. The horizontal dotted line indicates a zero slope and the vertical line the corresponding ξ_t. **c)** Solar Fe I abundance versus ξ_t. The vertical dotted line indicates the value for ξ_t that we adopt, and the horizontal line the corresponding solar Fe I abundance.

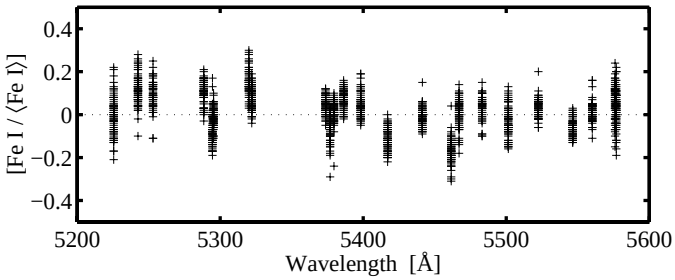

Fig. 9. Example of the difference between Fe I abundances derived from individual lines and the mean Fe I abundance. Each vertical distribution consists of $[\mathrm{Fe\,I}_\lambda/\langle\mathrm{Fe\,I}\rangle_\star]$ for up to 66 stars (all lines are not measured in all stars).

6. Atomic data

6.1. Oscillator strengths

6.1.1. General discussion

The abundance derived from a single spectral line is directly proportional to the oscillator strength, $\log gf$-value, for the transition (see e.g. Eq. (14.4) in Gray 1992). It is therefore of the highest priority to find $\log gf$-values that are as homogeneous and accurate as possible.

We are here faced with a choice between laboratory or astrophysically determined $\log gf$-values. Both have their advantages and disadvantages. Using laboratory data means that we have one parameter less that is dependent on the model atmosphere, i.e. the error in the $\log gf$-value is truly independent. This is valuable especially when analyzing stars that are not close to the Sun as regards stellar parameters, e.g. metal-poor giants in the halo. But, as discussed in e.g. Sikström et al. (2002), even if a $\log gf$-value has been determined using laboratory measurements, usually through measurements of lifetimes and branching fractions with a claimed high precision there are still uncertainties present.

Astrophysical $\log gf$-values are determined by requiring the equivalent widths, usually measured in a solar spectrum, to reproduce the standard solar abundance of that element. Other well-studied stars may also be used as reference. Using astrophysical $\log gf$-values will result in a truly differential study. This means that the internal errors in the study will be minimized and thus it is possible to find also small differences between stars. However, even though astrophysical $\log gf$-values give a very high internal consistency, comparisons with other studies become more difficult as another source of errors is included.

The aim with our analysis is to quantify any differences between F and G dwarf stars in the thin and thick disks. Therefore it might at first seem that astrophysical $\log gf$-values would be our natural choice. However, we also want to put our derived abundances on a baseline that is as general as possible as we want to compare with e.g. our own upcoming study of giant stars in the thick disk. It should also be noted that indeed all our stars are not solar like. The most metal-poor stars have for instance [Fe/H] ~ -1.

We therefore decided to investigate the possibility to use laboratory data in our analysis. This proved to be a most useful excursion and we indeed found that for many elements not only good but also homogeneous sets of laboratory data are available. Given our large number of lines we were also able to check certain corrections that have been suggested in previous studies (see Appendix B, and especially Fe I). But for a number of important α-elements and for Zn no good, homogeneous sets of laboratory data are available. We then chose to derive our own astrophysical $\log gf$-values.

In Appendix B we discuss, for each element and ion, the available laboratory data and the reasons for choosing astrophysical $\log gf$-values for certain cases. Table 3 lists our adopted $\log gf$-values. As starting points in our search for $\log gf$-values we used large data compilations such as VALD (Piskunov et al. 1995; Kupka et al. 1999), NIST Spectra Atomic Database (Martin et al. 1988; Fuhr et al. 1988), Kurucz Atomic Line Database (Kurucz & Bell 1995), and for Fe I Nave et al. (1994). However, all *original* sources have been checked, and Table 3 lists these references for the selected $\log gf$-values.

6.1.2. Consistency checks and calibration to standard solar abundances

After tuning the stellar parameters we checked for deviating abundances from individual lines in all stars. Spectral lines that produced abundances that deviated a lot from the mean abundance of all the lines from the same atom or ion were further

Table 3. Atomic line data. Columns 1 and 2 give the element and the degree of ionization (1 = neutral, 2 = singly ionized). Column 3 gives the wavelength (in Å), Col. 4 the lower excitation potential (in eV), Col. 5 the correction factor to the classical Unsöld damping constant, and Col. 7 the radiation damping constant. A "S" in Col. 6 indicates that the broadening by collisions have been taken from Anstee & O'Mara (1995), Barklem & O'Mara (1997, 1998), and Barklem et al. (1998, 2000), instead of the classical Unsöld broadening (indicated by an "U"). Column 8 gives our adopted $\log gf$-values and Col. 9 the references to the original sources. Astrophysical $\log gf$-values are indicated by "asterisks" in the reference column. The full table is available in electronic form at the CDS via anonymous ftp to `cdsarc.u-strasbg.fr (130.79.128.5)` or via `http://cdsweb.u-strasbg.fr/cgi-bin/qcat?J/A+A/410/527`.

El.	Ion	λ (Å)	χ_1 (eV)	$\delta\gamma_6$	DMP	$\gamma_{\rm rad}$ (s^{-1})	$\log gf$	Ref.
Al	1	5557.07	3.14	2.50	U	3.0e+08	−2.21	*
Al	1	6696.03	3.14	2.50	U	3.0e+08	−1.63	*
Al	1	6698.67	3.14	2.50	U	3.0e+08	−1.92	*
⋮	⋮	⋮	⋮	⋮	⋮	⋮	⋮	⋮

Table 4. Solar elemental abundances. Column 1 indicate the elements and ions and Cols. 2 and 3 give the meteoritic and solar photospheric standard abundances from Grevesse & Sauval (1998). Our solar abundances are given in Cols. 4 and 5 gives the differences between this study and the photospheric values. Asterisks indicate that we have used astrophysical $\log gf$-values and thereby forced the abundance to the standard photospheric value. Asterisks in parenthesis indicate that some of the lines have astrophysical $\log gf$-values.

Ion	Meteorites	Photosphere	This study	Diff.
Fe I	7.50	7.50	7.56	+0.06
Fe II	7.50	7.50	7.58	+0.08
Na I	6.32	6.33	6.27	−0.06
Mg I	7.58	7.58	7.58	*
Al I	6.49	6.47	6.47	*
Si I	7.56	7.55	7.54	−0.01(∗)
Ca I	6.35	6.36	6.36	*
Ti I	4.94	5.02	4.92	−0.10
Ti II	4.94	5.02	4.91	−0.11
Cr I	5.69	5.67	5.67	*
Cr II	5.69	5.67	5.67	*
Ni I	6.25	6.25	6.24	−0.01(∗)
Zn I	4.67	4.60	4.60	*

investigated. In Fig. 9 we give an example for Fe I, where we plot [Fe I_λ/⟨Fe I⟩$_\star$] for 32 lines in the interval 5200–5600 Å for all 66 stars. Fe I_λ is the abundance from a specific Fe I line and ⟨Fe I⟩$_\star$ the mean abundance from all measured Fe I lines.

Ideally a spread around zero is expected, representing the errors in the derived stellar parameters as well as the measurements of the equivalent widths and the placement of continua.

The reasons why a specific line deviates in all stars from the mean abundance can be several. A too high abundance can be caused by blends, incorrect $\log gf$-values, or blends by telluric lines. However, since the stars have different radial velocities some stars would be affected by telluric lines and some not. Hence the star-to-star scatter would be large. In the case of a blend by another stellar line the star-to-star scatter should be smaller. The smallest scatter should be expected for incorrect $\log gf$-values as all stars are equally affected. For a too low abundance, relative to the mean, the most likely cause of the deviation is an incorrect $\log gf$-value. A final cause for both too high and too low abundances are incorrect measurements of the equivalent widths, in particular the placement of the continuum. We do, however, believe this error to be rather negligible and reasonably well understood (see Sect. 7.1.1).

For Fe I and Fe II we rejected all lines that, for all stars, showed a large deviation in the same direction. Other elements were treated similarly.

Table 4 lists the solar abundances we derive. As can be seen they are in reasonable agreement with the standard photospheric abundances from Grevesse & Sauval (1998), but there are cases when the agreement is less good. Such disagreements could be caused by erroneous $\log gf$-values. However, as discussed in Appendix B there are good reasons to believe that many of the laboratory $\log gf$-values are of high quality. We have therefore choosen to keep the homogeneous sets of laboratory $\log gf$-values and instead apply a correction term to the stellar abundances. The correction term is the difference between Cols. 3 and 4 in Table 4. Effectively this could be viewed as overall correction terms to the $\log gf$-values (see also discussion in Chen et al. 2000). For elements where only astrophysical $\log gf$-values have been used there are, obviously, no correction terms. In Table 6 we give the corrected abundances.

6.2. Atomic line broadening

The broadening of atomic lines by radiation damping was considered in the determination of abundances. Radiation damping constants ($\gamma_{\rm rad}$) for the different lines were collected from Kurucz & Bell (1995).

Collisional broadening, or van der Waals broadening, was also considered. The width cross-sections are taken from Anstee & O'Mara (1995), Barklem & O'Mara (1997, 1998), and Barklem et al. (1998, 2000). Lines present in these studies have been marked by an "S" in Table 3. For spectral lines not present in these studies (marked by a "U" in Table 3) we apply the correction term ($\delta\gamma_6$) to the classical Unsöld approximation of the van der Waals damping, which for most elements were set to 2.5, following Mäckle et al. (1975). For Fe I we take the correction terms from Simmons & Blackwell (1982), but for Fe I lines with a lower excitation potential greater than 2.6 eV we follow Chen et al. (2000) and adopt a value of 1.4. For Fe II we adopt a constant value of 2.5 (Holweger et al. 1990).

For stronger lines the effect on the abundances of including the new collisional broadening cross-sections can be large. Therefore it is difficult to compare our astrophysical $\log gf$-values to those in the literature that were published prior to the appearance of the studies cited above. Our astrophysical Ni I $\log gf$-values, for example, do not compare at all to the ones in Edvardsson et al. (1993) although the measured

Table 5. Estimates of the effects on the derived abundances due to internal (random) errors for four stars. When calculating $\Delta W_\lambda/\sqrt{N}$ we have assumed ΔW_λ = 5% for Hip 88622, Hip 3142, and Hip 118115, and ΔW_λ = 10% for Hip 103682, see Sect. 7.1.1. The total random errors ($\sigma_{\rm rand}$) were calculated assuming the individual errors to be uncorrelated. The final line gives the average of the total random error for the four stars.

	[X/H]			[X/Fe I]											[X/Mg I]						
	Fe I	Fe II	Mg I	Na I	Mg I	Al I	Si I	Ca I	Ti I	Ti II	Cr I	Cr II	Ni I	Zn I	Na I	Al I	Si I	Ca I	Ti I	Ti II	Zn I
Hip 88622																					
$\Delta T_{\rm eff}$ = +70 K	0.06	−0.01	0.04	−0.02	−0.02	−0.04	−0.04	−0.01	0.07	−0.05	−0.01	−0.08	−0.02	−0.03	0.00	−0.02	−0.02	0.01	0.03	−0.03	−0.01
$\Delta \log g$ = +0.1	−0.01	0.04	−0.02	−0.01	−0.01	−0.01	0.00	−0.01	0.00	0.04	0.01	0.04	0.00	0.00	0.00	0.00	0.01	0.00	0.01	0.05	0.01
$\Delta\xi_{\rm t}$ = +0.15 km s^{-1}	−0.02	−0.02	−0.01	0.02	0.01	0.01	0.01	0.01	0.00	0.00	0.01	0.00	0.00	−0.01	0.01	0.00	0.00	0.00	−0.01	−0.01	−0.02
Δ[Fe/H] = +0.1	0.01	0.02	0.01	−0.01	0.00	−0.01	0.00	0.01	−0.01	0.02	0.00	0.01	0.00	0.02	−0.01	−0.01	0.00	0.01	−0.01	0.02	0.02
$\Delta\delta\gamma_6$ = +50%	0.00	−0.03	−0.06	−0.01	−0.06	−0.01	−0.04	−0.01	0.00	−0.04	0.00	−0.03	0.00	−0.06	0.05	0.05	0.02	0.05	0.06	0.02	0.00
$\Delta W_\lambda/\sqrt{N}$	0.00	0.00	0.01	0.01	0.01	0.01	0.00	0.00	0.00	0.00	0.01	0.01	0.00	0.01	0.00	0.00	−0.01	−0.01	−0.01	−0.01	0.00
$\sigma_{\rm rand}$	0.06	0.06	0.08	0.03	0.07	0.05	0.06	0.02	0.07	0.08	0.02	0.09	0.02	0.07	0.05	0.05	0.03	0.05	0.07	0.07	0.03
Hip 3142																					
$\Delta T_{\rm eff}$ = +70 K	0.05	−0.01	0.03	−0.01	−0.02	−0.03	−0.03	−0.01	0.01	−0.04	0.00	−0.05	0.00	−0.01	0.01	−0.01	−0.01	0.01	0.03	−0.02	0.01
$\Delta \log g$ = +0.1	0.00	0.03	−0.01	−0.01	−0.01	−0.01	0.00	−0.02	0.00	0.03	0.00	0.04	0.00	−0.01	0.00	0.00	0.01	−0.01	0.01	0.04	0.00
$\Delta\xi_{\rm t}$ = +0.15 km s^{-1}	−0.02	−0.03	−0.01	0.01	0.01	0.01	0.01	−0.01	0.01	−0.01	0.01	0.00	0.01	−0.02	0.00	0.00	0.00	−0.02	0.00	−0.02	−0.03
Δ[Fe/H] = +0.1	0.00	0.01	0.00	0.01	0.00	0.00	0.00	0.00	0.00	0.01	0.00	0.01	0.00	0.01	0.01	0.00	0.00	0.00	0.00	0.01	0.01
$\Delta\delta\gamma_6$ = +50%	0.00	−0.02	−0.02	0.00	−0.02	0.00	−0.02	−0.01	0.00	−0.03	0.00	−0.03	0.00	−0.02	0.02	0.02	0.00	0.01	0.02	−0.01	0.00
$\Delta W_\lambda/\sqrt{N}$	0.00	0.00	0.01	0.01	0.01	0.01	0.00	0.00	0.00	0.00	0.01	0.01	0.00	0.01	0.00	0.00	−0.01	−0.01	−0.01	−0.01	0.00
$\sigma_{\rm rand}$	0.05	0.05	0.04	0.02	0.03	0.03	0.03	0.03	0.01	0.06	0.01	0.07	0.01	0.03	0.02	0.02	0.02	0.03	0.04	0.05	0.03
Hip 118115																					
$\Delta T_{\rm eff}$ = +70 K	0.05	−0.02	0.03	−0.01	−0.02	−0.03	−0.04	0.00	0.02	−0.05	0.00	−0.06	0.00	−0.03	0.01	−0.01	−0.02	0.02	0.04	−0.03	−0.01
$\Delta \log g$ = +0.1	−0.01	0.04	−0.02	−0.01	−0.01	−0.01	0.00	−0.02	0.00	0.04	0.00	0.05	0.01	0.01	0.00	0.00	0.01	−0.01	0.01	0.05	0.02
$\Delta\xi_{\rm t}$ = +0.15 km s^{-1}	−0.04	−0.03	−0.01	0.03	0.03	0.03	0.03	0.01	0.01	0.01	0.02	0.01	0.02	0.00	0.00	0.00	0.00	−0.02	−0.02	−0.02	−0.03
Δ[Fe/H] = +0.1	0.01	0.03	0.01	0.00	0.00	−0.01	0.00	0.00	−0.01	0.02	−0.01	0.02	0.00	0.02	0.00	−0.01	0.00	0.00	−0.01	0.02	0.02
$\Delta\delta\gamma_6$ = +50%	0.00	−0.03	−0.07	−0.02	−0.07	−0.02	−0.04	−0.01	0.01	−0.03	0.00	−0.03	0.00	−0.06	0.05	0.05	0.03	−0.06	0.08	0.04	−0.01
$\Delta W_\lambda/\sqrt{N}$	0.00	0.00	0.01	0.01	0.01	0.01	0.00	0.00	0.00	0.00	0.01	0.01	0.00	0.01	0.00	0.00	−0.01	−0.01	−0.01	−0.01	0.00
$\sigma_{\rm rand}$	0.06	0.07	0.08	0.04	0.08	0.05	0.06	0.02	0.03	0.07	0.02	0.08	0.02	0.07	0.05	0.05	0.04	0.07	0.09	0.08	0.04
Hip 103682																					
$\Delta T_{\rm eff}$ = +70 K	0.05	−0.02	0.03	−0.02	−0.02	−0.02	−0.03	0.00	0.02	−0.05	0.00	−0.07	0.00	−0.03	0.00	0.00	−0.01	0.02	0.04	−0.03	−0.01
$\Delta \log g$ = +0.1	−0.01	0.03	−0.03	−0.02	−0.02	−0.01	0.00	−0.02	0.01	0.05	0.00	0.04	0.01	0.00	0.00	0.01	0.02	0.00	0.03	0.07	0.02
$\Delta\xi_{\rm t}$ = +0.15 km s^{-1}	−0.05	−0.04	−0.02	0.03	0.03	0.04	0.03	0.02	0.02	0.02	0.03	0.01	0.02	0.00	0.00	0.01	0.00	−0.01	−0.01	−0.01	−0.03
Δ[Fe/H] = +0.1	0.00	0.03	0.01	0.01	0.01	0.01	0.02	0.01	0.00	0.04	0.00	0.02	0.01	0.04	0.00	0.00	0.01	0.00	−0.01	0.03	0.03
$\Delta\delta\gamma_6$ = +50%	0.00	−0.03	−0.07	−0.02	−0.07	−0.03	−0.05	−0.02	0.00	−0.03	0.00	−0.03	−0.01	−0.06	0.05	0.04	0.02	0.05	0.07	0.04	0.01
$\Delta W_\lambda/\sqrt{N}$	0.00	0.01	0.02	0.02	0.02	0.02	0.01	0.01	0.01	0.01	0.01	0.01	0.00	0.03	0.00	0.00	−0.01	−0.01	−0.01	−0.01	0.01
$\sigma_{\rm rand}$	0.07	0.07	0.09	0.05	0.08	0.06	0.07	0.04	0.03	0.09	0.03	0.09	0.03	0.08	0.05	0.04	0.03	0.06	0.09	0.09	0.05
$\langle\sigma_{\rm rand}\rangle$	0.06	0.06	0.07	0.03	0.06	0.05	0.05	0.03	0.03	0.07	0.02	0.08	0.02	0.06	0.04	0.04	0.03	0.05	0.07	0.07	0.04

equivalent widths for the same lines are in good agreement (see Fig. 4).

7. Errors in resulting abundances

7.1. Internal random errors

7.1.1. Equivalent widths

Undetected blends, telluric lines, or artefacts caused by the reduction process are examples of features that can distort a spectral line so that it gives an erroneous W_λ. We have been observant of strangely shaped lines and rejected them from further analysis.

Stellar rotation ($v \sin i$) poses no major problem as long as it is mild. It simply broadens the spectral lines in a manner such that the total line strengths are unaffected. One possible effect is that faint lines might be smeared out and disappear and in crowded regions lines can be difficult to resolve. A few stars that were observed had to be rejected in the analysis due to high values of $v \sin i$ (Hip 238, 13679, 17651, 20284, 24162, 85397, 86736, 96556, 102485, 104680, 109422, and 115713).

The major source of error is actually not distortions of the line, but the placement of the stellar continuum. For spectral lines at shorter wavelengths, and especially in metal-rich stars, this possibility is higher than for lines located in uncrowded parts of the spectra, or for stars at lower metallicities. From our FEROS spectra we estimate that a maximum error of 5% in the measured W_λ is typical for most stars. In the worst cases, in very crowded parts of the spectra, we estimate a maximum error of 10% in the measured equivalent widths due to the misplacement of continua.

The precision by which an equivalent width is determined also depends on the signal-to-noise ratio in the spectrum. The error in W_λ due to the S/N can be estimated using the relationship from Cayrel (1989):

$$\sigma(W_\lambda) \sim 1.6\,\frac{\sqrt{FWHM \cdot \Delta x}}{S/N}, \qquad (6)$$

where $FWHM$ (in Å) is the width of the spectral line, Δx is the dispersion (in Å pixel^{-1}), and S/N is the signal-to-noise ratio. For a rather weak line ($W_\lambda \simeq 15$ mÅ) at $\lambda \sim 5000$ Å ($\Delta x \simeq 0.033$ Å pixel^{-1} in our FEROS spectra) with $FWHM = 0.15$ Å in a spectrum with $S/N = 150$ its equivalent width is measured with a precision of ∼0.7 mÅ according to this formula, or in other words with an uncertainty of ∼5%. The influence of low S/N is smaller for stronger lines, e.g. for $W_\lambda \simeq 100$ mÅ with $FWHM \simeq 0.19$ Å the precision becomes ∼0.8 mÅ or <1%.

For stronger lines ($W_\lambda \gtrsim 100$ mÅ) there is a potential problem with the actual fitting procedure. Sometimes a Gaussian line profile does not match the observed line profile whereupon

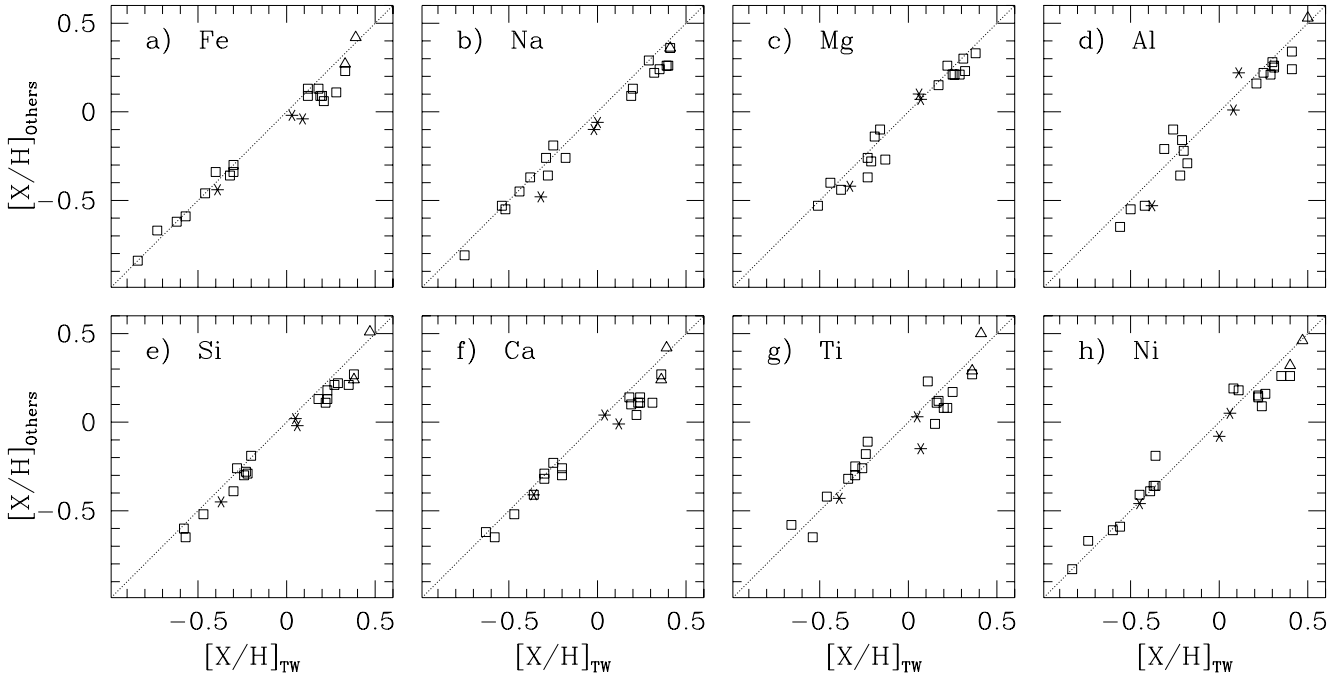

Fig. 10. Comparison of abundances to [Fe/H] to Edvardsson et al. (1993) (□), Feltzing & Gustafsson (1998) (△), and Chen et al. (2000) (∗). The elements are indicated in the plots. Dotted lines indicate the 1:1 relationships and values from this work, $[X/H]_{TW}$, are always plotted on the abscissas.

we instead fitted a Voigt profile. This selection was made by eye. We have in general good agreement between abundances from weaker and stronger lines, which encourage us to believe that a misjudgment is not particularly common.

In summary, we estimate our measured equivalent widths to have an average uncertainty of $\lesssim$5% for stars with low or moderate metallicities and maybe up to 10% for stars with [Fe/H] $\gtrsim$ 0.1. This amounts to 0.02–0.04 dex in the abundance determination from individual lines. For an element represented by N lines these estimates should be decreased by a factor $\sqrt{N}$ to give the formal error in the mean of the abundance based on those lines. These errors are exemplified in Table 5.

7.1.2. Atomic data

As is seen in Fig. 9 there are discrepancies between abundances even if they are derived with $\log gf$-values that are believed to be of high accuracy. However, the uncertainty of the mean abundance decreases as $1/\sqrt{N}$ where N is the number of lines. For an abundance derived from many lines the formal error in the mean arising from uncertainties in the atomic parameters is therefore often negligible.

The damping constants are usually associated with large uncertainties, but the effects on the derived abundances are normally small. We estimate a maximum influence by increasing the adopted enhancement factors by 50% (see Table 5). However, this estimate only applies to those lines for which the collisional broadening was derived by the classical Unsöld approximation (marked by an "U" in Table 3).

7.1.3. $T_{\rm eff}$ and $\xi_{\rm t}$

A change in $T_{\rm eff}$ with ±200 K affected the [Fe/H] vs. χ_1 plot by an amount that was easily recognizable, as was a change of ±0.3 km s^{-1} in the $\xi_{\rm t}$, easily discernible in the plot of [Fe/H] vs. log(W_λ/λ). These values can therefore be taken to represent the absolute maximum errors of these two atmospheric parameters under the assumption of LTE. If errors have a Gaussian distribution within these limits a reasonable estimate of the (1σ) uncertainties would be $\sigma(T_{\rm eff}) \simeq 70$ K and $\sigma(\xi_{\rm t}) \simeq 0.10$ km s^{-1}. To ensure that we do not underestimate the errors we used $\sigma(T_{\rm eff}) \simeq 100$ K and $\sigma(\xi_{\rm t}) \simeq 0.15$ km s^{-1} when doing the calculations for Table 5.

7.1.4. $\log g$

We determined the surface gravities through parallaxes and hence the uncertainty is dependent on the uncertainties of the parameters in Eq. (4), i.e. $\mathcal{M}$, $T_{\rm eff}$, π, and BC. The maximum relative error of the parallaxes in our sample is 4.4%, $\sigma(T_{\rm eff}) \simeq 70$ K, and we estimate that $\sigma(\mathcal{M}) \simeq 20\%$ and $\sigma(BC) \simeq 0.05$ mag. This translates into an internal (random) uncertainty in $\log g$ of ~0.08 dex. In the calculations for Table 5 we used $\sigma(\log g) = 0.1$ to make sure that we are not too optimistic when estimating the uncertainties of the stellar masses and the bolometric corrections.

7.1.5. Summing of random errors

In Table 5 the effect on derived abundances from the random errors discussed above are tabulated for four of our stars. There is

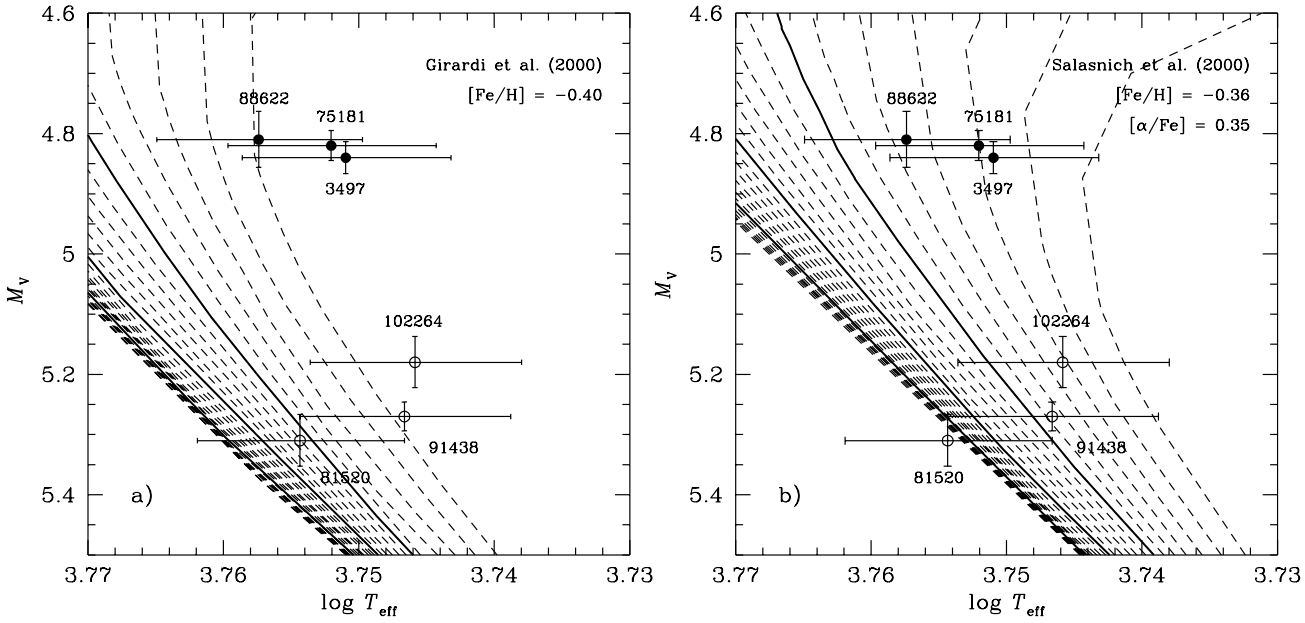

Fig. 11. Examples of age estimates. In **a)** we show the Girardi et al. (2000) isochrones for [Fe/H] = −0.40 and in **b)** the Salasnich et al. (2000) isochrones for [Fe/H] = −0.36 and an α-enhancement of [α/Fe] = 0.35. The ages that the isochrones represent are ..., 2, 2.2, 2.5, 2.8, 3.2, 3.5, 4.0, 4.5, 5.0, 5.6, 6.3, 7.1, 7.9, 8.9, 10, 11.2, 12.6, 14.1, 15.9, 17.8, and 19.9 Gyr (the last one only for Salasnich et al. 2000). Isochrones for 2, 5, and 10 Gyr are marked by solid lines. The stars in the plots have metallicities in the interval −0.55 < [Fe/H] < −0.20. Thick and thin disk stars are marked by filled and open circles, respectively. Horizontal error-bars represent the 100 K uncertainty in $T_{\rm eff}$ and the vertical error-bars the individual errors in the parallaxes.

one thin disk and one thick disk star at [Fe/H] ∼ −0.4 and two thin disk stars are at [Fe/H] = 0 and [Fe/H] = +0.3, respectively. The main contributors to the total error are the uncertainties in $T_{\rm eff}$ and $\xi_{\rm t}$, where the latter error is clearly increasing with metallicity. This trend is mainly due to the fact that lines that are closer to saturation in the line cores (more common in metal-rich stars) have a strong dependence on $\xi_{\rm t}$.

Typical values on the total random error are ≈0.05 dex for Hip 88622 and Hip 3142 and ≈0.07 dex for Hip 103682 with Hip 118115 lying in between. The average values of the total random errors from these four stars are also given in the bottom line of Table 5.

7.2. Comparison with other studies – systematic errors

Systematic errors are more difficult to quantify. By comparing atmospheric parameters and derived abundances to already published values it is however possible to see if there are offsets present. In Fig. 10 we compare our derived abundances for stars that we have in common with Edvardsson et al. (1993), Feltzing & Gustafsson (1998), and Chen et al. (2000). There is generally good agreement with no particular trends. Small offsets might however be present when comparing to individual studies.

Also the atmospheric parameters, $T_{\rm eff}$ and $\log g$, show good agreement for the stars in common with Edvardsson et al. (1993), Feltzing & Gustafsson (1998), and Chen et al. (2000).

8. Ages

Stellar ages were determined using isochrones from Girardi et al. (2000) for stars with no α-enhancement and isochrones (with [α/Fe] ≃ 0.35) from Salasnich et al. (2000) for stars with α-enhancements. The chemical compositions of the different sets of isochrones were translated to [Fe/H]-metallicities using (Bertelli et al. 1994)

$$[\mathrm{Fe/H}] = 1.024 \cdot \log Z + 1.739, \quad (7)$$

for the Girardi et al. (2000) isochrones, and (L. Girardi 2001, private comm.)

$$[\mathrm{Fe/H}] = \log(Z/0.019) - \log(X/0.708) - 0.3557, \quad (8)$$

for the Salasnich et al. (2000) isochrones. In the equations, X and Z are the H and "metal" abundance fractions, respectively, which together with the He fraction, Y, add up to 1. Examples of our age determinations are shown in Figs. 11a, b for 6 stars that have metallicities in the range −0.55 < [Fe/H] < −0.20. The impact of considering α-enhanced isochrones is obvious. As an approximate dividing limit we treated stars with [Mg/Fe] $\gtrsim$ 0.1 as being α-enhanced. For stars within ±0.05 dex of this limit we determined ages from both sets of isochrones and adopted the mean value. Lower and upper age limits were estimated from the end points of the errors bars representing the uncertainties in the stellar parallaxes and $T_{\rm eff}$ (see Fig. 11). The final columns in Table 2 give these lower and upper limits and the most probable ages. Table 2 also indicates which sets of isochrones were used. Stars that are not sufficiently evolved, i.e. still on the main sequence, do not have age estimates.

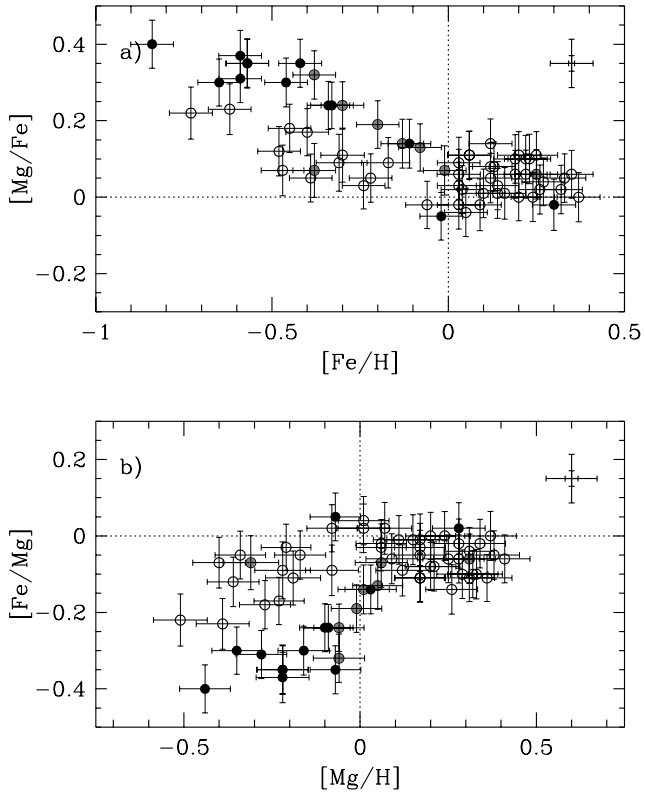

Fig. 12. Magnesium abundances. The error bar in top right corner gives both the average formal error in the mean and the average total error (see Sect. 9). Individual error bars give the total error. Thin disk stars are marked by empty circles and thick disk stars by filled (black: TD/D > 10, grey: 1 < TD/D < 10) circles.

We find average ages of 4.9±2.8 Gyr and 11.2±4.3 Gyr for the thin and thick disks, respectively. In Feltzing et al. (2003) we quoted slightly higher average ages of 6.1±2.0 Gyr and 12.1±3.8 Gyr for the same thin and thick disk stellar samples. Those ages were taken from Feltzing et al. (2001) who did not use α-enhanced isochrones, which in general give lower ages than isochrones without α-enhancements. Note also that here we use the spectroscopic $T_{\rm eff}$ s, which for individual stars can have an impact. However, the mean ages of the two populations are still separated.

9. Abundance results

Our abundance results are shown in Figs. 12, 13 and 15 where we plot abundances relative to Fe and Mg. The error bars that are shown in the top right hand corner of these plots represent two different types of errors. The smallest error-bar represents the average of the formal error in the mean ($\langle\sigma_{\rm form}\rangle$) from all stars. The formal error in the mean is given by $\sigma_{\rm form} = \sigma_{\rm lines}/\sqrt{N_{\rm lines}}$, where $\sigma_{\rm lines}$ is the line-to-line scatter (see e.g. Gray 1992, page 444). The larger represents the total internal error in our study and is given by $\sigma_{\rm tot} = \sqrt{\langle\sigma_{\rm form}\rangle^2 + \langle\sigma_{\rm rand}\rangle^2}$, where $\langle\sigma_{\rm rand}\rangle$ is given on the last row in Table 5. In Fig. 12 we also show the $\sigma_{\rm tot}$ for individual stars.

In some cases we derive abundances from both the atom and the ion of the element. In the plots we have used the average of Ti I & Ti II for Ti and the average of Cr I & Cr II for Cr in order to increase the statistics. The abundance trends do not change when using the mean values as compared to using the different ions separately. There is, however, lower scatter in the plots when the average values are used. For Fe we used the abundances from Fe I only since the number statistics are large.

All abundances have been normalized with respect to the standard solar photospheric abundances as given in Grevesse & Sauval (1998) (see Table 4 and discussion in Sect. 6 and Appendix B).

9.1. Abundances as a function of [Fe/H]

9.1.1. The α-elements

The three key results for the α-elements in our study are:

1. Below [Fe/H] = 0 the thin and thick disks show clearly distinct abundance trends (see Figs. 12a, and 13c–e). This difference is statistically robust, and, as is seen in Fig. 12a, there is no overlap of the distributions even when uncertainties in the derived abundances are considered.
2. The presence of supernovae type Ia (hereafter SN Ia) signatures in the thick disk. Starting with an overabundance of [α/Fe] = 0.3–0.4 at [Fe/H] $\simeq -0.8$, and remaining flat until [Fe/H] $\simeq -0.4$, the thick disk [α/Fe] trend then declines toward the solar values. This behaviour is interpreted as being due to the time delay between the supernovae type II (hereafter SN II) and the long-lived SN Ia in the enrichment of the interstellar medium.
3. Quiet evolution in the thin disk. Abundance trends show shallow declines when going from slight overabundances of [α/Fe] = 0.1–0.2 at [Fe/H] $\simeq -0.7$ until reaching solar values at [Fe/H] = 0. The "knee" that we see in e.g. the [Mg/Fe] trend for the thick disk does not appear in the thin disk. This is indicative of a lower star-formation rate (see e.g. McWilliam 1997).

Our first finding is a confirmation of Fuhrmann (1998), who for Mg found the thin and thick disks to be chemically disjunct. The signature of SN Ia in the thick disk has also recently been indicated in the study by Mashonkina & Gehren (2001) in their analysis of Ba and Eu abundances in a local stellar sample.

For [Fe/H] > 0 the spread is remarkably low for [Si/Fe] and [Ti/Fe]. This is a significant improvement compared to previous studies (notably Edvardsson et al. 1993; Feltzing & Gustafsson 1998).

At [Fe/H] > 0 the number of thick disk stars in our sample is small. Whether they truly are members of the thick disk or not is further discussed in Sect. 9.4.

9.1.2. Sodium and aluminum

McWilliam (1997) noted, from a phenomenological point of view, that Al and perhaps Na could be classified as mild α-elements, even though their nuclei have odd numbers of protons.

Al behaves, relative to Fe, *exactly* as an α-element, Fig. 13b. We also reproduce the upward trend in [Al/Fe] at

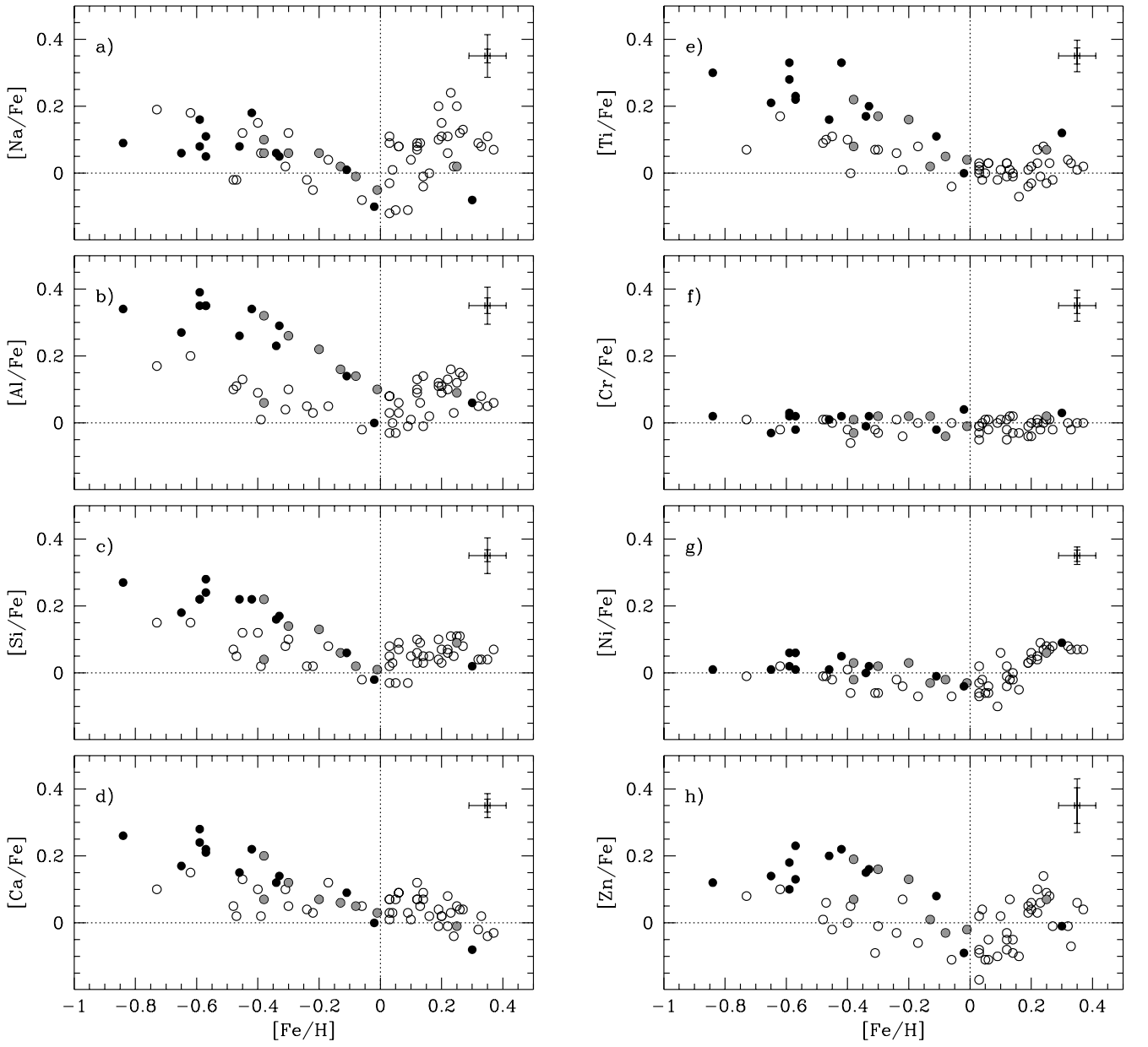

Fig. 13. Elemental abundances relative to Fe. Dotted lines indicate solar values. The error bar give both the average formal error in the mean and the average total error, see Sect. 9. For the thin and thick disk subsamples at [Fe/H] < 0 in the Cr and Ni trends we performed linear regressions. The slopes (k) and the zero-point constants (m) are: $k_{\rm thin} = -0.02 \pm 0.04$, $m_{\rm thin} = -0.02 \pm 0.01$ and $k_{\rm thick} = -0.02 \pm 0.03$, $m_{\rm thick} = 0.00 \pm 0.01$ for Cr, and $k_{\rm thin} = -0.12 \pm 0.04$, $m_{\rm thin} = -0.08 \pm 0.02$ and $k_{\rm thick} = -0.08 \pm 0.03$, $m_{\rm thick} = -0.02 \pm 0.01$ for Ni. Thin disk stars are marked by empty circles and thick disk stars by filled (black: TD/D > 10, grey: 1 < TD/D < 10) circles.

[Fe/H] > 0 seen in Edvardsson et al. (1993) and Feltzing & Gustafsson (1998).

The [Na/Fe] trend is not as clear as that of Al (compare Figs. 13a and 13b). The distributions of the two stellar populations have a more "merged" appearance. Thick disk stars show a shallow rise or a flat trend from solar abundances to [Na/Fe] $\simeq$ 0.1 at [Fe/H] $\simeq -0.4$ where it levels out and continues at a constant value to lower metallicities. For [Fe/H] > 0 there is a rise in the [Na/Fe] trend, which was also seen in Feltzing & Gustafsson (1998) and Edvardsson et al. (1993) but there it was slightly less pronounced.

Both Na and Al can be subject to NLTE effects. For recent discussions see Baumüller et al. (1998) and Baumüller & Gehren (1997). In general the effects on the abundances tend to be that they are too high if they are derived under the assumption of LTE. However, the effects become severe only for metallicities below [Fe/H] = −1 and/or for temperatures greater than $T_{\rm eff} = 6500$ K. At solar values the effects are usually negligible. Given the $T_{\rm eff}$s and [Fe/H]s of our stars we did not consider the NLTE effects in the determination of our Na and Al abundances, and furthermore, the effects would have been small.

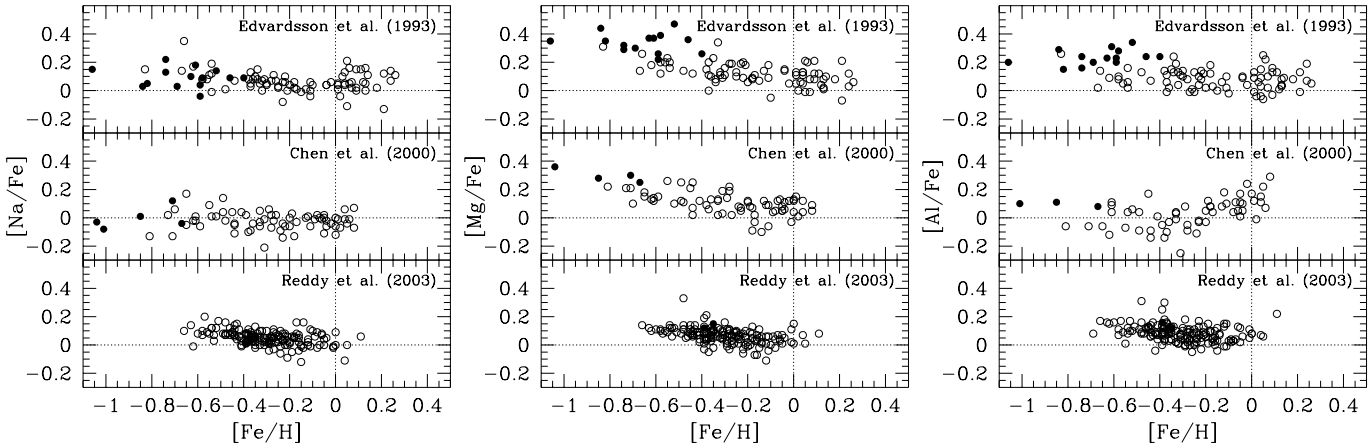

Fig. 14. Na, Mg, and Al abundances for stars from Edvardsson et al. (1993), and Chen et al. (2000). The stars are selected according to the criteria that we have used for thin and thick disk membership in our sample, Sect. 2. Thick and thin disk stars are marked by filled and open circles, respectively. For a discussion see Sect. 9.1.3.

9.1.3. Mg, Al, and Na – comparisons with other studies

In Fig. 14 we have taken the abundance data from the three studies Edvardsson et al. (1993), Chen et al. (2000), and Reddy et al. (2003) and applied our kinematic selection criteria to their samples. New galactic velocity components were calculated, using Hipparcos data and radial velocities from Barbier-Brossat et al. (1994), for the Edvardsson et al. (1993) stars. For the Reddy et al. (2003) and the Chen et al. (2000) stars we adopted their published $U_{\rm LSR}$, $V_{\rm LSR}$, and $W_{\rm LSR}$ velocities. Thin and thick disk stars were then selected in the same manner as in Sect. 2, i.e. TD/D ≤ 0.1 and TD/D ≥ 10 for the thin and the thick disks, respectively.

The Edvardsson et al. (1993) stars were originally selected to, in each [Fe/H] bin, sample different parts of the velocity space. This means that we should expect their sample to contain both thin and thick disk stars. Since metal-poor ($\lesssim -0.6$ dex) thin disk stars and metal-rich ($\gtrsim -0.4$ dex) thick disk stars are rare we could expect these parts of the disks to be poorly sampled. These preconceptions are born out in the three Edvardsson et al. (1993) plots in Fig. 14. The trends in their and our data are (where the distributions overlap) the same. We note that the internal accuracy in Edvardsson et al. (1993) should be lower when compared with our study as they use, in most cases, significantly fewer spectral lines.

When applying our kinematic selection criteria to the Chen et al. (2000) sample we get a small and rather scattered sample of thick disk stars. However, if we view the scatter in the data as due to internal errors we can conclude that the overall trend in the thin disk agrees roughly with ours (allowing for extra scatter in the Al thin disk data) and that the thick disk data is not, within the errors, inconsistent with our trends.

Finally, we apply our selection criteria to the Reddy et al. (2003) data. Their sample was originally selected to trace the chemical evolution in the thin disk below solar metallicity. Our selection criteria give 163 of their stars as thin disks stars and 2 stars as thick disk stars. Our thin disk trends nicely agree with theirs. We note that the thick disk stars follow the thin disk trend.

9.1.4. Even Z iron peak

Cr is an iron peak element that has been found to vary in lockstep with Fe (e.g. Edvardsson et al. 1993; Feltzing & Gustafsson 1998; Chen et al. 2000). Our abundance trends do not present any novelties concerning Cr apart from that it shows an extremely tight trend with a potential shallow decline (see Fig. 13f).

Ni is usually found to show a solar value of [Ni/Fe] for all [Fe/H] (e.g. Edvardsson et al. 1993; Feltzing & Gustafsson 1998; Chen et al. 2000). We find, however, that [Ni/Fe] shows a slight overabundance at the lowest metallicities and, at [Fe/H] > 0, an increase in [Ni/Fe] that is different to previous studies (see Fig. 13g). This rise in [Ni/Fe] at [Fe/H] > 0 will have an impact on the observed [O/Fe] trend when oxygen abundances are derived from the forbidden oxygen line at 6300 Å as this line has a Ni blend (see Johansson et al. 2003; Bensby et al. 2003a,b). The overall scatter in the [Ni/Fe] trend is low.

For both Cr and Ni we see a potential offset between the thin and thick disk subsamples at [Fe/H] < 0, with the thick disk being more enhanced. These offsets could be further strengthened by linear regressions (see caption of Fig. 13) but considering the internal errors in our data these offsets are marginally significant. Larger stellar samples would be needed to confirm them.

9.1.5. Zinc

The [Zn/Fe] trend is shown in Fig. 13h. At [Fe/H] < 0 the thin and thick disk trends are distinct. The thick disk stars show overabundances that resemble those of the α-elements. Thin disk stars have roughly [Zn/Fe] = 0, although with a slight negative slope at higher [Fe/H]. At metallicities above solar there is a pronounced rise in [Zn/Fe]. The previous major studies of Galactic Zn abundances are Sneden et al. (1991) and

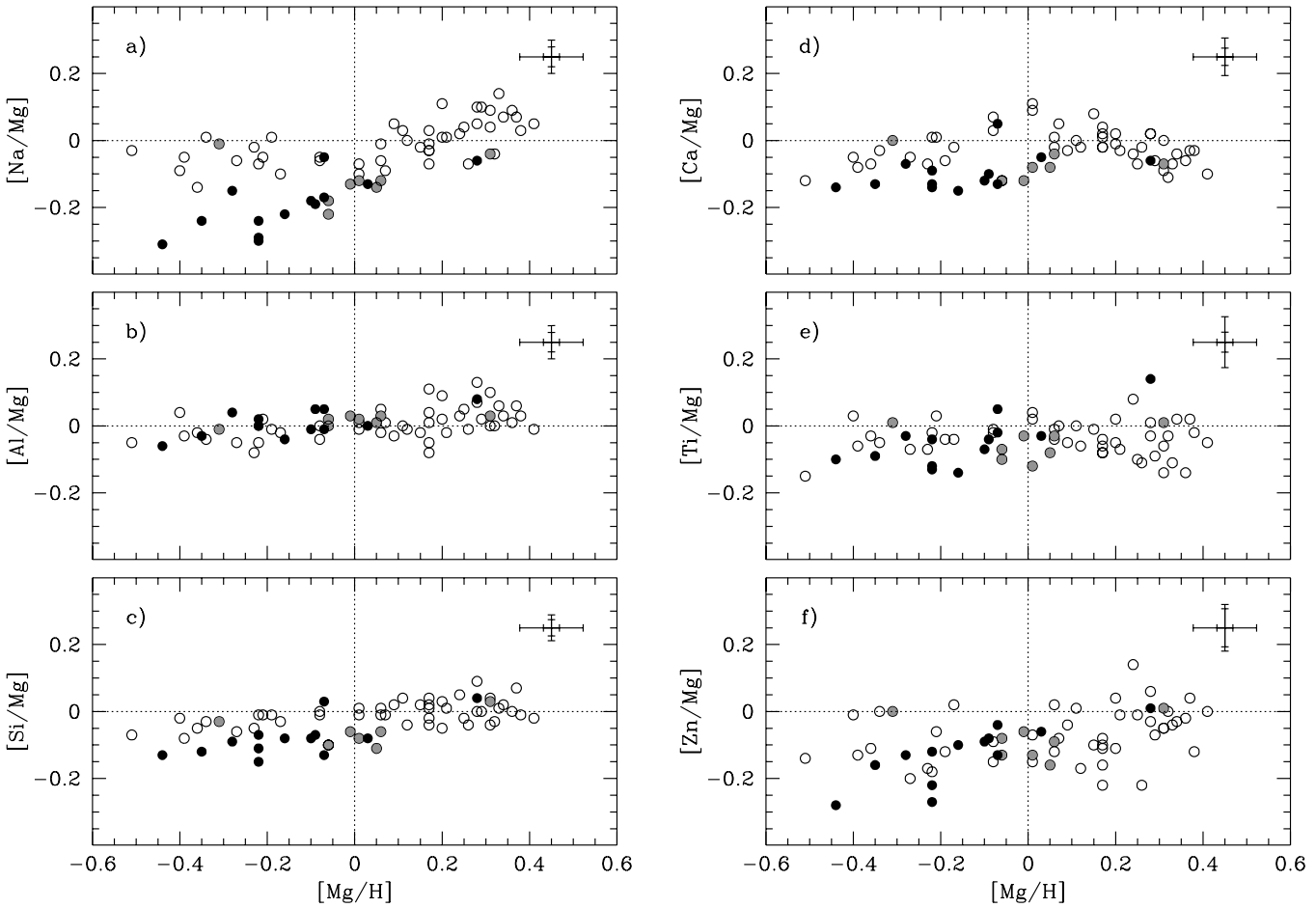

Fig. 15. Elemental abundances relative to Mg. Dotted lines indicate solar values. The error bar give both the average formal error in the mean, and the average total error, see Sect. 9. Thin disk stars are marked by empty circles and thick disk stars by filled (black: TD/D > 10, grey: 1 < TD/D < 10) circles.

Mishenina et al. (2002). These studies concentrated on stars spanning the metallicity range $-3 <$ [Fe/H] < -0.1 and they found that Zn abundances closely track the overall metallicities, but with a slight overabundance of [Zn/H] $\sim +0.04$. Prochaska et al. (2000) find for their 10 thick disk stars an overabundance of [Zn/Fe] in concordance with our results. Our uprising [Zn/Fe] trend at [Fe/H] > 0 is, to our best knowledge, new. There is, however, a possibility that the uprising trend could be somewhat overestimated (see Appendix B).

9.2. Abundances as a function of [Mg/H] – Implications for nucleosynthesis

After investigating different elemental abundances, all compared to Fe, it is illustrative to make comparisons to an element such as Mg. This element is believed to be solely produced by SN II, see e.g. Arnett (1996) and Woosley & Weaver (1995), while Fe is produced by both SN Ia and SN II (e.g. Thielemann et al. 2002). Especially for the other α-elements, Si, Ca, and Ti, such comparisons can lead to further understanding of the events in which these elements are synthesized, i.e. SN II vs. SN Ia contributions.

Due to a lower star-formation rate the time scales for the enrichment of the interstellar medium in the thin disk are longer than for the thick disk. Also, as the thin disk forms and evolves, embedded in the thick disk, it could be influenced by SN Ia that emerge from the thick disk population. These two things will make the observed abundance trends in the thin disk more difficult to interpret.

9.2.1. Iron

In Fig. 12b we plot the "inverse" of Fig. 12a, i.e. [Fe/Mg] versus [Mg/H]. The upward trend in [Fe/Mg], that is a signature of the onset of the contribution from SN Ia to the chemical enrichment of the interstellar medium, is seen for the thick disk at [Mg/H] ~ -0.1. At lower Mg abundances [Fe/Mg] is mainly flat, corresponding to an epoch where SN II are the only contributors to the Fe enrichment.

For the thin disk at [Mg/H] < 0 there is a shallow rise towards the solar value. Since Mg is only produced in SN II the observed trend must be interpreted as due to Fe enrichment from SN Ia.

Above [Mg/H] = 0 the [Fe/Mg] trend for the thin disk is essentially flat. Most models of galactic chemical evolution are normally not evolved much beyond the Sun. This makes the exact interpretation of the abundance patterns above solar difficult. However, it appears that the production of Mg and Fe reaches an equilibrium for [Mg/H] > 0, indicating that contributions from SN Ia and SN II are equal.

9.2.2. α-elements

Ca, Si, and Ti are all made in SN II. According to SN Ia models they should also be made in these events (e.g. Thielemann et al. 2002). Given the interpretation of the Fe and Mg trends we can now use our data to check if a discernible fraction of these elements are also produced in SN Ia.

We see a flat [Si/Mg] trend for the thick disk while for [Ca/Mg] we see an upward trend at [Mg/H] ~ 0 (see Figs. 15c, d). For Ti the scatter is too large for any trends to be deciphered (see Fig. 15e). The [Ca/Mg] trend in the thick disk support the idea that an observable amount of Ca is also produced in SN Ia (compare Fe, Sect. 9.2.1). This is of course a tentative result that needs to be confirmed with future studies.

The thick disk [Si/Mg] trend implies that no Si is produced in SN Ia, i.e. the trend remains flat to the highest [Mg/H]. However, this appears to be contradictory to nucleosynthesis models of SN Ia (e.g. Thielemann et al. 2002) which show Si to be produced in significant amounts in these events.

A first interpretation for the [Ca/Mg] trend in the thin disk is that it first increases due to Ca enrichment by SN Ia (compare the discussion for Fe in Sect. 9.2.1). The reason for the subsequent down-turn at higher [Mg/H] could have several reasons. One interpretation could be that the SN Ia rate reaches a peak around or slightly after [Mg/H] = 0 and after that SN II dominate the enrichment more and more. Alternatively, SN yields become metallicity-dependent at super-solar metallicities.

9.2.3. Sodium and aluminium

Na and Al are results of Ne and C burning in massive stars that later become SN II (see e.g. Arnett 1996). For Al this explanation is supported by our abundance trends. Since Mg is a sole product of SN II the flat [Al/Mg] trend in Fig. 15b indicates that Mg and Al have similar origins.

The [Na/Mg] trends for the two populations separate nicely (see Fig. 15a). For the thin disk we have [Na/Mg] ≈ 0, with some scatter and an upward trend at [Mg/H] > 0. The thick disk [Na/Mg] trend shows large under-abundances at the lowest [Mg/H] and then steadily rises with increasing [Mg/H]. The interpretation of these trends is unclear. They might have implications for the effect on yields from the mass cut off in SN explosions.

9.2.4. Zinc

The resemblance of the Zn abundance trend to that of the α-elements is weaker when it is compared to Mg rather than Fe (compare Figs. 13 and 15). From this it is clear that the nucleosynthetic origin of Zn is not as clear as e.g. for Si. According to Mishenina et al. (2002) roughly 1/3 of the Zn yields comes from primary processes in massive stars (SN II) and 2/3 from SN Ia. Given the spread in the data this is compatible with our results since we see a gentle rise in the [Zn/Mg] for all [Mg/H] which is indicative of contributions from both SN Ia and SN II. We also note that the [Zn/Mg] trend is fairly similar to the [Na/Mg] trend in Fig. 15a.

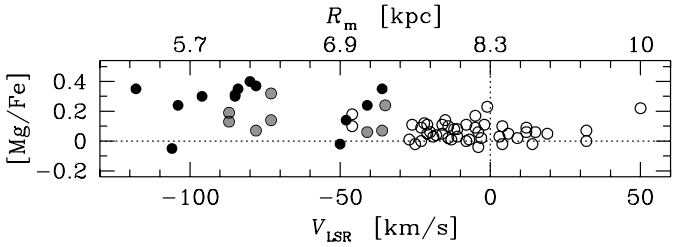

Fig. 16. [Mg/Fe] vs. V_{LSR}, with R_m indicated on the top axis of the plot. Thin disk stars are marked by empty circles and thick disk stars by filled (black: TD/D > 10, grey: 1 < TD/D < 10) circles.

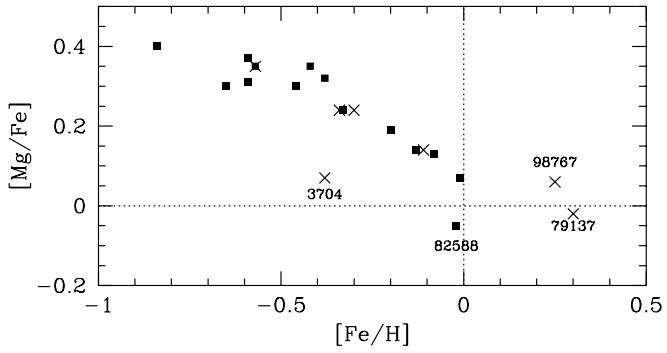

Fig. 17. [Mg/Fe] vs. [Fe/H] for the thick disk sample. Stars with $V_{LSR} < -60$ km s^{-1} are marked by solid squares, and those with $V_{LSR} > -60$ km s^{-1} with crosses. The stars discussed in Sect. 9.4 are marked by their Hipparcos numbers.

9.3. Velocities and abundances

9.3.1. Different galactocentric radii

To check if the abundance trends we see for the whole thick disk sample are the same irrespective of birthplace in the Galaxy we make use of the tight correlation between galactocentric distance (R_m) and the V_{LSR} space velocity component (Edvardsson et al. 1994). R_m is calculated as the mean value of the apo- and perigalactic distances of the stellar orbits in a given model potential.

Figure 16 shows [Mg/Fe] versus V_{LSR} and it so happens that our thick disk sample has two main groupings, which also can be seen in Fig. 3; one around $V_{LSR} \simeq -40$ km s^{-1} and one around $V_{LSR} \simeq -80$ km s^{-1} or $\langle R_m \rangle \sim 7.0$ kpc and $\langle R_m \rangle \sim 6.0$ kpc. The innermost sample should have a minimum of contamination of thin disk stars with thick disk kinematics.

Figure 17 shows the [Mg/Fe] vs. [Fe/H] trends with the thick disk sample split into the two velocity groups. We have

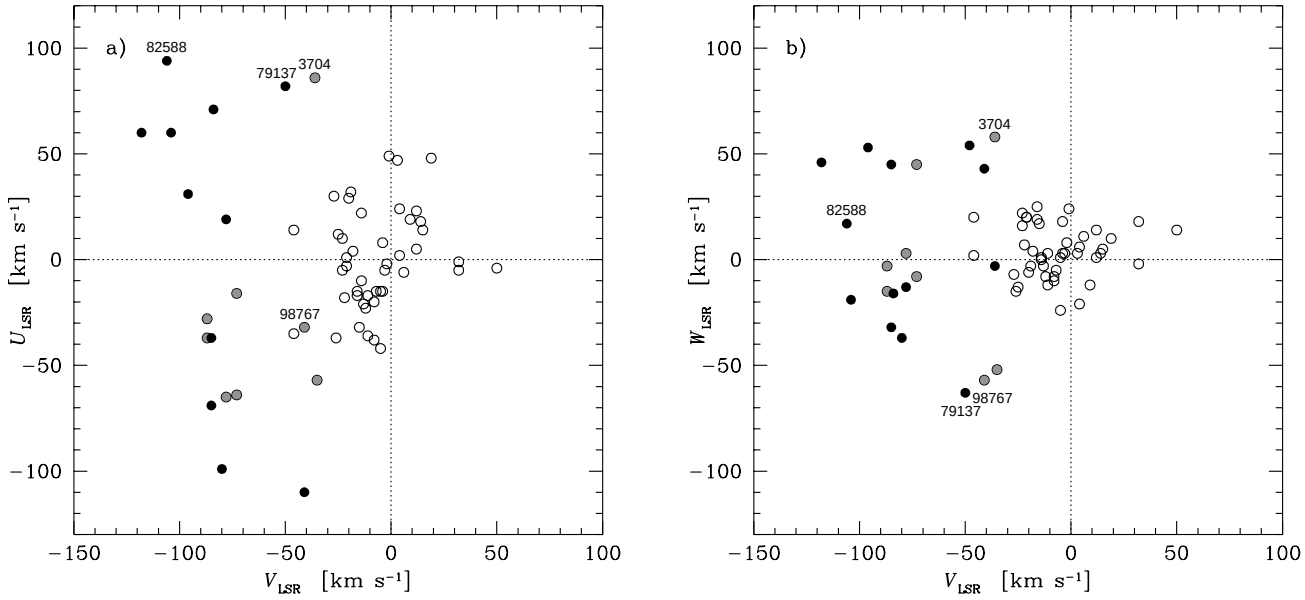

Fig. 18. Galactic $U_{\rm LSR}$ and $W_{\rm LSR}$ velocities versus $V_{\rm LSR}$. Four thick disk stars are marked by their Hipparcos numbers, see Sect. 9.4. Thin disk stars are marked by empty circles and thick disk stars by filled (black: TD/D > 10, grey: 1 < TD/D < 10) circles.

a well defined abundance trend for the stars with $V_{\rm LSR} < -60$ km s^{-1} (filled squares). The trend is the same for the stars with $V_{\rm LSR} > -60$ km s^{-1} although not as well sampled (crosses). Also, the one deviating thick disk star (Hip 3704) is in the sample with the larger $\langle R_{\rm m} \rangle$ and can thus readily be attributed to thin disk contamination (see Sect. 9.4).

9.3.2. Thick disk stars with 1 < TD/D < 10

Thick disk stars that were selected with relaxed criteria 1 < TD/D < 10, see Sect. 2, do follow the same abundance trends as thick disk stars with TD/D > 10, see Figs. 12, 13, and 15, indicating that the dividing limits we set for the thin and thick disks (TD/D < 0.1 and TD/D > 10, respectively) are by no means definite.

9.4. Deviating stars

Based on their α-element abundances and kinematics there are four thick disk stars that merit further discussion. These stars are marked by their Hipparcos numbers in Figs. 3, 17, and 18.

The thick disk star Hip 82588 has a large $U_{\rm LSR}$ velocity and a low $W_{\rm LSR}$ velocity (see Figs. 18a and b). This implies a shallow elongated galactic orbit. Its $V_{\rm LSR}$ velocity (-106 km s^{-1}) gives a galactocentric radius of ~5.5 kpc (compare Fig. 16). Hip 82588 could therefore possibly be attributed to the inner disk or be a nearby bulge-like star (e.g. Pompéia et al. 2002). The thick disk stars Hip 3704 and Hip 79137 both have high $U_{\rm LSR}$ and $W_{\rm LSR}$ velocities. This means that they have elongated orbits but also that they reach high above the galactic plane. This makes them likely thick disk stars. However, Hip 3704 has typical thin disk abundances, see Fig. 17, which makes it a prime candidate for a thin disk star that has had its orbit perturbed by a molecular cloud, or close encounter with another star, or it could have been expelled from a binary system. Hip 98767 has a low $U_{\rm LSR}$ velocity and a high $W_{\rm LSR}$ velocity which gives a typical thick disk orbit.

9.5. Age trends

Figures 19a and b show the stellar ages, see Sect. 8, as functions of [Fe/H] and $V_{\rm LSR}$. Within the uncertainties there is no evidence that the $V_{\rm LSR} < -60$ km s^{-1} thick disk subsample ($\langle$Age$\rangle$ = 9.9 ± 4.0 Gyr) is older than the $V_{\rm LSR} > -60$ km s^{-1} subsample ($\langle$Age$\rangle$ = 11.8 ± 4.6 Gyr).

The mean age for the metal-poor ([Fe/H] < 0) thin disk stars are, within the uncertainties, equal to the mean age of the metal-rich ([Fe/H] > 0) thin disk stars ($\langle$Age$\rangle$ = 5.7 ± 2.6 Gyr and $\langle$Age$\rangle$ = 4.7 ± 2.8 Gyr, respectively).

10. Clues to the formation of the thick disk

The various possible formation scenarios for the thick disk were discussed in the Introduction. We will now summarize the observational constraints and discuss the most likely formation scenario for the thick (and thin) disk.

10.1. Observational constraints

I. Distinct and smooth trends at [Fe/H] < 0: For [Fe/H] < 0 we find that the thin and thick disk abundance trends are clearly separated (see Sect. 9). Not only for the α-elements, but also for other elements such as Al and to a lesser extent Ni and Cr. These findings should rule out any model that predicts the two disks to form a continuous distribution. It is therefore most likely that the thin and thick disks have formed at epochs that are clearly separated in time and/or space.

The abundance trends we see are also well defined and smooth with small overall scatter. This is indicative of both the

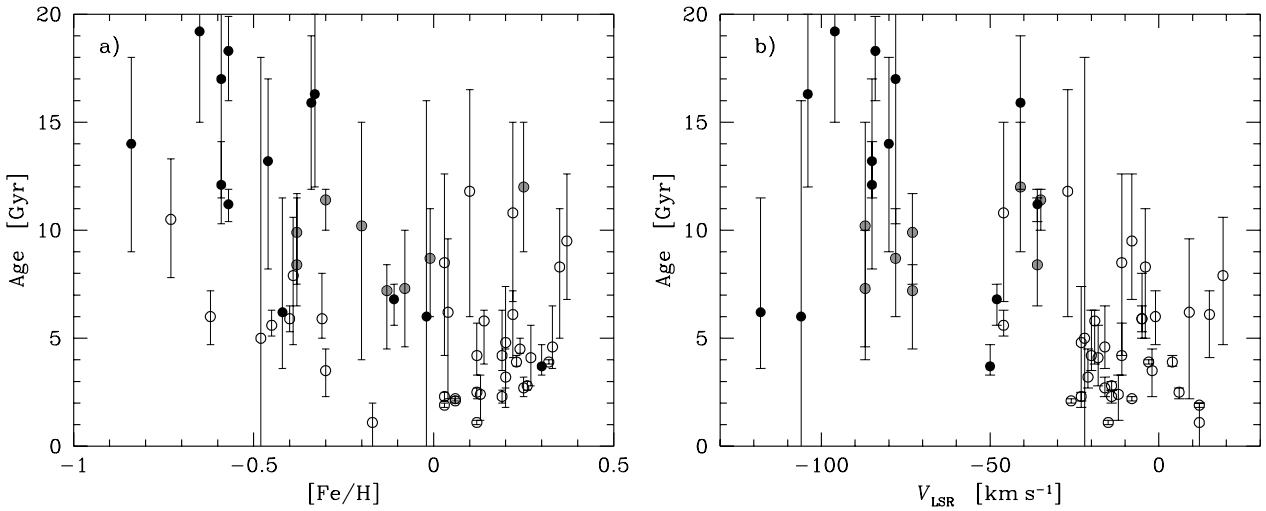

Fig. 19. a) Stellar ages versus [Fe/H] and **b)** versus V_{LSR}. The error-bars represent the lowest and highest possible ages inferred by the errors introduced by parallaxes and effective temperatures in the fitting of the isochrones, see Fig. 11, Sect. 8, and Table 2. Thin disk stars are marked by empty circles and thick disk stars by filled (black: TD/D > 10, grey: 1 < TD/D < 10) circles.

thin and thick disks having formed from interstellar gas that was reasonably well mixed.

II. SN Ia in the thick disk: That we see such a clear and well defined signature from SN Ia in the thick disk indicates that the gas from which it formed must have been chemically homogeneous. Star formation must also have continued in the thick disk after the serious onset of SN Ia since we see thick disk stars with [Fe/H] > -0.4 that have formed from interstellar gas with a lower [α/Fe].

This means that the star formation rate in the thick disk must initially have been fast to allow the build-up of α-elements from SN II to high metallicities before the enrichment from SN Ia. The horizontal position of the "knee" sets a lower limit to how long the star formation went on for in the thick disk. An often quoted time-scale for SN Ia to contribute to the chemical enrichment is one billion years. However, depending on the star formation rate this time-scale might be shorter. In e.g. Matteucci (2001) it is shown how, in a bursting scenario, the SN Ia rate peaks after only a few hundred million years, i.e. significantly earlier.

III. Ages: We find that our thick disk sample is on average older than our thin disk sample, 11.2 ± 4.3 Gyr and 4.9 ± 2.8 Gyr, respectively (see Sect. 8). This indicates that the thin and thick disks formed at separate time epochs.

IV. Vertical gradients: The lack of vertical abundance gradients in the thick disk (Gilmore et al. 1995). This indicates that the thick disk formed on a reasonably short time scale. If not, gradients would have had time to build up (compare Burkert et al. 1992). The evidence is based on observations of two stellar samples at distances of 1 kpc and 1.5 kpc from the galactic plane, respectively.

V. Extra-galactic evidence: In a study of 110 edge-on spiral galaxies Schwarzkopf & Dettmar (2000) found that thick disks are much more common under conditions where the host galaxies are in merging/interacting environments. Their sample consisted of 69 non-interacting galaxies and of 49 interacting galaxies/minor merging candidates. The disk scale heights for perturbed disks were found to be ∼1.5 times larger than for galaxies having unperturbed disks. Also Reshetnikov & Combes (1997) found the scale height of interacting galaxies to be two times higher than for isolated galaxies. Their sample consisted of 29 edge-on interacting spiral galaxies and 7 edge-on isolated galaxies. This indicates that thick disks are more likely to be present if the host galaxies are in environments where they are gravitationally influenced by other galaxies.

10.2. The most likely scenario

The observational evidence that we have presented in this study, i.e. constraints I to III presented above, favours a formation scenario for the thick disk that produces smooth abundance trends that are distinct and well separated between the thin and the thick disks. This should also be the case for the age distributions in the two disks. The scenarios that fulfill this are the fast and the slow dissipational collapses and the merging/interacting scenarios (see e.g. Gilmore et al. 1989, and Sect. 1). Other evidence that can be found in the literature puts the merging/interacting scenarios at advantage to the dissipational ones. Constraint IV e.g. rules out a slow dissipational collapse and constraint V indicates that thick disks are common in merging/interacting scenarios. Taking all this evidence together makes the merging scenario the most likely.

The merger scenario has been modelled with N-body simulations (e.g. Quinn et al. 1993; Walker et al. 1996; Huang & Carlberg 1997; Velázquez & White 1999). Although the full consequences of a merger event are not yet fully understood it is clear that some heating will occur. In order to inflate the old

Table 6. Derived abundances relative hydrogen, [X/H], where X denotes the different elements as indicated. Each element has three columns, mean abundance ([X/H]), standard deviation of the mean abundance ($\sigma_{[X/H]}$), and the number of spectra lines (N) that has been used in computing the mean abundance. The abundances have been normalized with respect to the solar photospheric abundances as given in Grevesse & Sauval (1998), see also Table 4. The second column indicates if the star belongs to the thin disk (mem = 1) or the thick disk (mem = 2) (mem = 3 indicates the Sun). The full table is available in electronic form at the CDS via anonymous ftp to `cdsarc.u-strasbg.fr (130.79.128.5)` or via `http://cdsweb.u-strasbg.fr/cgi-bin/qcat?J/A+A/410/527`.

	mem	Fe I			Fe II			Na I			Mg I			...
		[X/H]	$\sigma_{[X/H]}$	N_{lines}	[X/H]	$\sigma_{[X/H]}$	N_{lines}	[X/H]	$\sigma_{[X/H]}$	N_{lines}	[X/H]	$\sigma_{[X/H]}$	N_{lines}	...
Sun	3	0.00	0.09	147	0.00	0.09	29	0.00	0.04	4	0.00	0.00	7	...
Hip 3086	2	−0.11	0.09	145	−0.18	0.07	24	−0.10	0.03	4	0.03	0.05	6	...
Hip 3142	1	−0.45	0.09	131	−0.45	0.08	25	−0.33	0.04	4	−0.27	0.05	7	...
⋮	⋮	⋮	⋮	⋮	⋮	⋮	⋮	⋮	⋮	⋮	⋮	⋮	⋮	⋱

thin disk to the velocity dispersions that today's thick disk exhibits, the simulations indicate that the merging galaxy has to be quite massive (~0.1–0.2 of the Milky Way disk). We note that dwarf galaxies in the Local Group with masses of that order are rare (see e.g. Mateo 1998).

11. Summary

In this paper we have presented a detailed abundance analysis of 66 F and G dwarf stars located in the solar neighbourhood. The stellar sample was kinematically selected with two subsamples representative of the thin and thick disks. In order to fully disentangle the chemical properties of the thin and thick disks we selected the samples on purely kinematical grounds. We have merely strived for an equal number of thin and thick disk stars in each metallicity bin below [Fe/H] = 0. All stars have been observed with the same telescope, using the same settings, the same reduction procedures, and abundances have been derived with exactly the same atomic parameters and model atmospheres. This enables a very robust differential comparison of the chemical evolution of the thin and thick disks with minimal internal uncertainties.

We find that the abundance trends in the thin and thick disks are distinct and well separated. For the α-elements the thick disk shows signatures of the onset of chemical enrichment to the interstellar medium from SN Ia. No such fossil record was found in the thin disk, which indicates its more quiet evolution. Previously it is only in the study by Mashonkina & Gehren (2001) that the SN Ia signature in the thick disk has been indicated.

Further we find that there exist stars with thick disk kinematics at [Fe/H] > 0. In general these stars follow the abundance trends outlined by the thin disk stars. However, some of them have Galactic orbits with high ellipticity and whether or not they truly belong to the thick disk or any other stellar subsystem (such as the Bulge) remains unclear.

We propose that a merging/interacting scenario for the thick disk is the most likely. This conclusion rests on two facts: that thick disks are more common in galaxies that are in merging/interacting environments; that there is no evidence for a vertical abundance gradient in the Galactic thick disk. As discussed the extra-galactic evidence is continuously growing while the Galactic evidence is based on only one study. We think that the most important future observational investigation would be to confirm the lack of a vertical abundance gradient in the thick disk.

We have performed an extensive investigation of the atomic data, $\log gf$-values in particular, that we used in the determination of the stellar abundances. However, we sometimes had to rely on astrophysical $\log gf$-values. In particular we note that in the optical region, good laboratory data is missing for many elements (e.g. Si, Mg, and Al), and that the Ca I $\log gf$-values draught from Smith & Raggett (1981) do not reproduce the solar abundances. The discrepancy that usually is found between abundances from Ti I and Ti II is not reproduced in this study. We find good consistency, which for the Sun is in concordance with the standard *meteoritic* value in Grevesse & Sauval (1998).

In the same observing runs as we obtained the FEROS spectra we also observed the faint forbidden oxygen line at 6300 Å for the same stars with the Coudé Echelle Spectrograph (CES) on the ESO 3.6 m telescope. With a resolving power exceeding 210 000 and a signal-to-noise above 400 these high quality spectra will enable accurate oxygen abundance determinations. First reports have been presented in Bensby et al. (2003a,b) and the full analysis will be presented in Bensby et al. (2003, submitted).

Acknowledgements. We would like to thank the developers of the Uppsala MARCS code, Bengt Gustafsson, Kjell Eriksson, Martin Asplund, and Bengt Edvardsson who we also thank for letting us use the *Eqwidth* abundance program. We also thank Bengt Edvardsson, Poul Erik Nissen, and Bengt Gustafsson for valuable comments on draft versions of the paper. TB thanks Kungliga Fysigrafiska Sällskapet i Lund for financial support to the first trip to La Silla in September 2000. SF is grateful for computer grants from the same society. This research has made use of the SIMBAD database, operated at CDS, Strasbourg, France.

Appendix A: Galactic velocity components

Galactic space velocity components were calculated by the following equation (L. Lindegren 2001, private comm.):

$$\begin{pmatrix} U_{\rm LSR} \\ V_{\rm LSR} \\ W_{\rm LSR} \end{pmatrix} = \begin{pmatrix} U_{\odot} \\ V_{\odot} \\ W_{\odot} \end{pmatrix} + \boldsymbol{G} \times \boldsymbol{R} \times \boldsymbol{X}, \quad \text{(A.1)}$$

where

$$\boldsymbol{G} = \begin{pmatrix} -0.0548756 & -0.8734371 & -0.4838350 \\ +0.4941094 & -0.4448296 & +0.7469822 \\ -0.8676661 & -0.1980764 & +0.4559838 \end{pmatrix}, \quad \text{(A.2)}$$

$$\boldsymbol{R} = \begin{pmatrix} -\sin\alpha & -\cos\alpha \cdot \sin\delta & \cos\alpha \cdot \cos\delta \\ \cos\alpha & -\sin\alpha \cdot \sin\delta & \sin\alpha \cdot \cos\delta \\ 0 & \cos\delta & \sin\delta \end{pmatrix}, \quad \text{(A.3)}$$

$$\boldsymbol{X} = \begin{pmatrix} C \cdot r \cdot \mu_{\alpha} \\ C \cdot r \cdot \mu_{\delta} \\ v_{\rm r} \end{pmatrix}, \quad \text{(A.4)}$$

and where α and δ denote the ICRS equatorial coordinates, μ_{α} and μ_{δ} the proper motions in [mas/yr], $v_{\rm r}$ the radial velocity in [km s^{-1}], $C = 4.74047$, r the distance in [pc], and $(U_{\odot}, V_{\odot}, W_{\odot}) = (+10.00, +5.25, +7.17)$ km s^{-1} that are the solar motions, relative the LSR, was taken from Dehnen & Binney (1998).

Appendix B: Oscillator strengths – remarks on individual elements

Aluminium: For our seven lines the first three have $\log gf$-values from Prochaska et al. (2000) (based on Buurman 1986). These give an average abundance 0.13 dex below the standard solar value. The other four lines have theoretically determined $\log gf$-values from Kurucz & Bell (1995) giving abundances 0.26 dex below the solar value. We chose to determine astrophysical $\log gf$-values.

Calcium: The major study on Ca I is Smith & Raggett (1981). Using their published $\log gf$-values we were however unable to reproduce the solar abundance. Chen et al. (2000) also used these oscillator strengths but had to adjust practically all the $\log gf$-values by subtracting ~0.1–0.2 dex in order to reproduce average abundances defined from selected stars. Our abundance from the lines where Smith & Raggett (1981) values were available give on average a value 0.17 dex below the standard solar value. We therefore chose to use our own astrophysical $\log gf$-values.

Chromium: Apart from two of our Cr I lines ($\lambda\lambda$ 4545.845, 5296.691 Å, Blackwell et al. 1984) we only found astrophysical $\log gf$-values (Kostyk 1981) and $\log gf$-values with uncited sources in the compilation by Fuhr et al. (1988). This combination of $\log gf$-values from the laboratory, the Sun, and by unknown methods lead us to abundances with a large dispersion and a solar abundance that was too low by 0.10 ± 0.09 dex.

For Cr II we only found astrophysical $\log gf$-values from Kostyk & Orlova (1983). We therefore made use of our own astrophysical $\log gf$-values for both Cr I and Cr II.

Iron: The Fe I lines from May et al. (1974), as listed in the compilation by Fuhr et al. (1988), have re-normalizing factors applied to the $\log gf$-values (-0.04 if $\log gf \geq -0.75$ and -0.10 if $\log gf < -0.75$). These corrections caused abundances from the May et al. (1974) lines to show overabundances in the Sun of 0.12 ± 0.09 dex (relative the mean abundance from all the lines). For the whole stellar sample differences varied between 0.07 and 0.13 dex (with an average value of 0.10 ± 0.01 dex) above the mean abundance from all Fe I lines for each star. We therefore adopted the *original* May et al. (1974) $\log gf$-values which give consistent results.

Our first source of $\log gf$-values for Fe II was the critical compilation by Giridhar & Ferro (1995). However, these represent an exotic mixture of different procedures for deriving $\log gf$-values. Raassen & Uylings (1998) have theoretically determined $\log gf$-values for thousands of Fe II lines. Comparisons in the UV to high quality measurements from the FERRUM project show them to be in excellent agreement with laboratory data, see for instance Karlsson et al. (2001) and Nilsson et al. (2000). By using the Raassen & Uylings (1998) oscillator strengths we obtained a homogeneous set of reliable $\log gf$-values for Fe II.

Compared to the standard Fe abundance from Grevesse & Sauval (1998) our solar abundances are slightly higher (see Table 4).

Magnesium: There were only theoretically determined $\log gf$-values for Mg I, Kurucz (1995). We used our own astrophysical $\log gf$-values.

Nickel: Kostyk (1982) $\log gf$-values were rejected as a source due to their astrophysical origin. Doerr & Kock (1985) and Lennard et al. (1975) were also rejected since they contained too few lines in common with our study. We instead choose the recently published $\log gf$-values from Wickliffe & Lawler (1997) whenever possible and our own astrophysical for the remaining lines. On average the Wickliffe & Lawler (1997) solar abundances are 0.09 dex too low compared to the standard Ni abundance from Grevesse & Sauval (1998). Since astrophysical $\log gf$-values are in the majority, among our lines, the derived solar abundance from all our lines are only 0.02 dex too low compared to Grevesse & Sauval (1998).

Silicon: Laboratory $\log gf$-values by Garz (1973) decreased by 0.10 dex, as recommended by Becker et al. (1980), were used when available. For the other lines we used our own astrophysical $\log gf$-values.

Titanium: Ti is an element that in its neutral form often is believed to give discrepancies due to NLTE effects, e.g. Luck & Bond (1985) found an average abundance from Ti I lines 0.16 ± 0.05 dex lower than if derived from Ti II lines.

Their Ti I abundances showed a clear temperature dependence while there was none or little dependence for the Ti II abundances. Prochaska et al. (2000) found that Ti II abundances exceeded the Ti I abundances by ~0.10–0.15 dex for all their stars. Their solar Ti abundance derived from Ti I was 4.89 and from Ti II 5.05. Also Stephens & Boesgaard (2002), who used $\log gf$-values from Bizzarri et al. (1993) and the compilation by Martin et al. (1988), got $\langle$[Ti I/Ti II]$\rangle = -0.06 \pm 0.06$. Note, however, that they used the Ti I and Ti II abundances in the determination of their surface gravities.

Using laboratory $\log gf$-values from the studies of Blackwell et al. (1982a, 1982b, 1983, 1986) (corrected according to Grevesse et al. 1989) for Ti I and from Pickering et al. (2001) for Ti II we found solar abundances that are 0.10 dex too low for Ti I and 0.11 dex too low for Ti II when compared to the standard solar photospheric abundance, $\log \epsilon_{\odot} = 5.02$, from Grevesse & Sauval (1998). There is also good agreement between Ti I and Ti II abundances for all 69 stars ($\langle$[Ti I/Ti II]$\rangle = 0.00 \pm 0.04$). No trends of abundances with effective temperature, surface gravity, metallicity, or microturbulence were found for either Ti I, Ti II or the difference between the two, Figs. 7e–f.

The main difference between this study and previous studies is the choice of oscillator strengths for Ti II. We used the recently published data from Pickering et al. (2001), while e.g. Prochaska et al. (2000) mainly used two sources, Bizzarri et al. (1993) and Savanov et al. (1990), where the latter is a compilation of published data. For the 13 Ti II lines we have in common with Prochaska et al. (2000) the mean difference is -0.09 ± 0.09 with their $\log gf$-values giving higher abundances. This difference could explain the difference between their Ti I and Ti II abundances.

Since the abundances in our study from Ti I and Ti II are consistent, Figs. 7e–h, we believe that the atomic data we have used for Ti are correct and that Ti I might not suffer from NLTE effects (i.e. previous discrepancies were due to incorrect $\log gf$-values) in the temperature range spanned by our stars. A probable reason for our low solar abundance is that the photospheric standard Ti abundance might be erroneous. A value of $\epsilon(\mathrm{Ti})_{\odot} = 4.91$ is a better match to our observations and closer to the meteoritic value (see Table 4).

Zinc: We use astrophysical $\log gf$-values for Zn. Originally the Zn lines at $\lambda\lambda$ 4722, 4810, 6362 Å were used. The two lines at shorter wavelengths are quite strong and are located in crowded parts of the spectra. This makes them susceptible to blends. The line at 6367 Å is located in a part of the spectrum where the continuum is lowered by ozone depression. Placement of the local continuum for this line is, however, no problem. By comparing the abundances from the two lines at shorter wavelengths to the 6362 Å line we discovered the 4722 Å line to show a prominent increase when going to higher [Fe/H], Fig. B.1a. We interpret this increase as due to a blend (probably Fe I) that is growing with metallicity. The 4810 Å line shows different offsets to the 6362 Å line at sub- and super-solar [Fe/H], Fig. B.1b. There is, however, no indication of a gradual increase with metallicity, but rather an abrupt increase of the spread at [Fe/H] ~ 0. We therefore choose to keep the 4811 Å line in combination with the 6362 Å line for our Zn abundances. It should however be noted that our Zn abundances at [Fe/H] > 0 could be slightly too high.

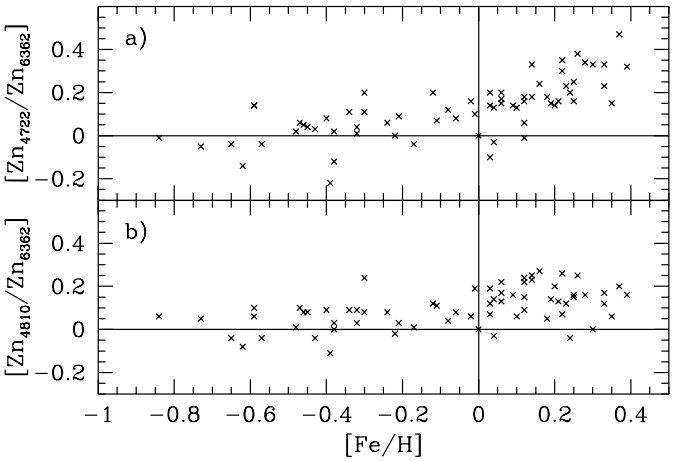

Fig. B.1. The difference between Zn abundances when derived from **a)** the $\lambda\lambda$4722, 6362 Å lines, and **b)** the $\lambda\lambda$4810, 6362 Å lines. The $\log gf$-values for all three lines are astrophysical.

References

Alonso, A., Arribas, S., & Martínez-Roger, C. 1995, A&A, 297, 197
Alonso, A., Arribas, S., & Martínez-Roger, C. 1996, A&A, 313, 873
Anstee, S. D., & O'Mara, B. J. 1995, MNRAS, 276, 859
Arnett, D. 1996, Supernovae and nucleosynthesis: an investigation of the history of matter from the big bang to the present (Princeton Series in Astrophysics, Princeton Academic Press)
Asplund, M., Gustafsson, B., Kiselman, D., & Eriksson, K. 1997, A&A, 318, 521
Barbier-Brossat, M., Petit, M., & Figon, P. 1994, A&AS, 108, 603
Barklem, P. S., & O'Mara, B. J. 1997, MNRAS, 290, 102
Barklem, P. S., & O'Mara, B. J. 1998, MNRAS, 300, 863
Barklem, P. S., O'Mara, B. J., & Ross, J. E. 1998, MNRAS, 296, 1057
Barklem, P. S., Piskunov, N., & O'Mara, B. J. 2000, A&AS, 142, 467
Baumüller, D., & Gehren, T. 1997, A&A, 325, 1088
Baumüller, D., Butler, K., & Gehren, T. 1998, A&A, 338, 637
Becker, U., Zimmermann, P., & Holweger, H. 1980, Geochim. Cosmoch. Acta, 44, 2145
Bensby, T., Feltzing, S., & Lundström, I. 2003a, ASP Conf. Ser. 304, CNO in the Universe, ed. C. Charbonnel D. Schaerer, & G. Meynet, in press [astro-ph/0212029]
Bensby, T., Feltzing, S., & Lundström, I. 2003b, Carnegie Observatories Astrophysics Series, vol. 4: Origin and Evolution of the Elements, ed. A. McWilliam and M. Rauch (Pasadena: Carnegie Observatories, http://www.ociw.edu/ociw/symposia/series/symposium4/proceedings.html) [astro-ph/0304182]
Bertelli, G., Bressan, A., Chiosi, C., Fagotto, F., & Nasi, E. 1994, A&AS, 106, 275
Bizzarri, A., Huber, M. C. E., Noels, A., et al. 1993, A&A, 273, 707
Blackwell, D. E., Menon, S. L. R., Petford, A. D., & Shallis, M. J. 1982a, MNRAS, 201, 611

Blackwell, D. E., Petford, A. D., Shallis, M. J., & Leggett, S. 1982b, MNRAS, 199, 21
Blackwell, D. E., Menon, S. L. R., & Petford, A. D. 1983, MNRAS, 204, 883
Blackwell, D. E., Menon, S. L. R., & Petford, A. D. 1984, MNRAS, 207, 533
Blackwell, D. E., Booth, A. J., Menon, S. L. R., & Petford, A. D. 1986, MNRAS, 220, 289
Burkert, A., Truran, J. W., & Hensler, G. 1992, ApJ, 391, 651
Buser, R., Rong, J., & Karaali, S. 1999, A&A, 348, 98
Buurman, E. P., Dönszelmann, A., Hansen, J. E., & Snoek, C. 1986, A&A, 164, 224
Cayrel, R. 1989, in The impact of very high S/N spectroscopy on stellar physics, ed. G. Cayrel de Strobel, & M. Spite (Dordrecht: Kluwer Academic Publ.), IAU Symp., 132, 345
Chen, B. 1997, ApJ, 491, 181
Chen, Y. Q., Nissen, P. E., Zhao, G., Zhang, H. W., & Benoni, T. 2000, A&AS, 141, 491
Chen, B., Stoughton, C., Allyn Smyth, J., et al. 2001, ApJ, 553, 184
Dalcanton, J. J., & Bernstein, R. A. 2002, AJ, 124, 1328
Dehnen, W., & Binney, J. J. 1998, MNRAS, 298, 387
Doerr, A., & Kock, M. 1985, J. Quant. Spectrosc. Radiat. Transfer, 33, 307
Edvardsson, B., Andersen, J., Gustafsson, B., et al. 1993, A&A, 275, 101
Edvardsson, B., Gustafsson, B., Nissen, P. E., et al. 1994, in Panchromatic view of galaxies. Their evolutionary puzzle, Proc. of the International Scientific Spring Meeting of the Astronomische Gesellschaft held in Kiel, Germany, March 8–12, 1993 (Gif-sur-Yvette: Éditions Frontières), ed. G. Hensler, C. Theis, & J.S. Gallagher, ESO, 401
ESA 1997, The Hipparcos and Tycho Catalogues, ESA SP-1200
Feltzing, S., & Gustafsson, B. 1998, A&AS, 129, 237
Feltzing, S., Holmberg, J., & Hurley, J. R. 2001, A&A, 377, 911
Feltzing, S., Bensby, T., & Lundström, I. 2003, A&A, 397, L1
Fuhr, J. R., Martin, G. A., & Wiese, W. L. 1988, J. Phys. Chem. Ref. Data, vol. 17, Suppl. 4, Atomic Transition Probabilities, Iron through Nickel
Fuhrmann, K. 1998, A&A, 338, 161
Fulbright, J. P. 2000, AJ, 120, 1841
Garz, T. 1973, A&A, 26, 471
Gilmore, G., & Reid, N. 1983, MNRAS, 202, 1025
Gilmore, G., Wyse, R. F. G., & Kuijken, K. 1989, ARA&A, 27, 555
Gilmore, G., Wyse, R. F. G., & Jones, J. B. 1995, AJ, 109, 3
Girardi, L., Bressan, A., Bertelli, G., & Chiosi, C. 2000, A&AS, 141, 371
Giridhar, S., & Ferro, A. A. 1995, Rev. Mex. Astron. Astrofis., 31, 23
Gray, D. F. 1977, ApJ, 218, 530
Gray, D. F. 1992, The observation and analysis of stellar photospheres, Cambridge Astrophysics Series 20 (Cambridge University Press)
Gratton, R. G., Carretta, E., Eriksson, K., & Gustafsson, B. 1999, A&A, 350, 955
Gratton, R. G., Carretta, E., Matteucci, F., & Sneden, C. 2000, A&A, 358, 671
Grevesse, N., & Sauval, A. J. 1998, Space Sci. Rev., 85, 161
Grevesse, N., Blackwell, D. E., & Petford, A. D. 1989, A&A, 208, 157
Gustafsson, B., Bell, R. A., Eriksson, K., & Nordlund, Å. 1975, A&A, 42, 407
Hakkila, J., Myers, J. M., Stidham, B. J., & Hartmann, D. H. 1997, AJ, 114, 2043
Hauck, B., & Mermilliod, M. 1998, A&AS, 129, 431
Holweger, H., Heise, C., & Kock, M. 1990, A&A, 232, 510
Huang, S., & Carlberg, R. G. 1997, ApJ, 480, 503
Johansson, S., Litzén, U., Lundberg, H., & Zhang, Z. 2003, ApJ, 584, L107
Karlsson, H., Sikström, C. M., Johansson, S., Li, Z. S., & Lundberg, H. 2001, A&A, 371, 360
Koen, C. 1992, MNRAS, 256, 65
Kostyk, R. I. 1981, Astrometriya Astrofiz., 45, 3
Kostyk, R. I. 1982, Astrometriya Astrofiz., 46, 58
Kostyk, R. I., & Orlova, T. V. 1983, Astrometriya Astrofiz., 49, 39
Kroupa, P. 2002, MNRAS, 330, 707
Kupka, F., Piskunov, N., Ryabchikova, T. A., Stempels, H. C., & Weiss, W. W. 1999, A&AS, 138, 119
Kurucz, R. L., & Bell, B. 1995, Atomic Line Data, Kurucz CD-ROM No. 23, Cambridge Mass., Smithsonian Astrophysical Observatory
Kurucz, R., Furenlid, I., Brault, J., & Testerman, L. 1984, Solar Flux Atlas from 296 to 1300 nm, National Solar Observatory, Sunspot, New Mexico
Lennard, W. N., Whaling, W., Scalo, J. M., & Testerman, L. 1975, ApJ, 197, 517
Livingston, W. C. 1999, Allen's Astrophysical Quantities, Fourth ed., ed. A.N. Cox (AIP, Springer-Verlag)
Luck, R. E., & Bond, H. E. 1985, ApJ, 292, 559
Mäckle, R., Holweger, H., Griffin, R., & Griffin, R., 1975, A&A, 38, 239
Martin, G. A., Fuhr, J. R., & Wiese, W. L. 1988, J. Phys. Chem. Ref. Data, vol. 17, Suppl. 3, Atomic Transition Probabilities, Scandium through Manganese
Mashonkina, L., & Gehren, T. 2001, A&A, 376, 232
Mateo, M. L. 1998, ARA&A, 36, 435
Matteucci, F. 2001, The Chemical Evolution of the Galaxy, Astrophysics and Space Science Library 253 (Kluwer Academic Publishers)
May, M., Richter, J., & Wichelmann, J. 1974, A&AS, 18, 405
McWilliam, A. 1997, ARA&A, 35, 503
Mishenina, T. V., Kovtyukh, V. V., Soubiran, C., Travaglio, C., & Busso, M. 2002, A&A, 396, 189
Moore, C. E., Minnaert, M. G. J., & Houtgast, J. 1966, The Solar Spectrum 2935 Å to 8770 Å, National Bureau of Standards Monograph 61
Nave, G., Johansson, S., Learner, R. C. M., Thorne, A. P., & Brault, J. W. 1994, ApJS, 94, 221
Nilsson, H., Sikström, C. M., Li, Z. S., et al. 2000, A&A, 362, 410
Pickering, J. C., Thorne, A. P., & Perez, R. 2001, ApJS, 132, 403
Piskunov, N. E., Kupka, F., Ryabchikova, T. A., Weiss, W. W., & Jeffery, C. S. 1995, A&AS, 112, 525
Pompéia, L., Barbuy, B., & Grenon, M. 2002, ApJ, 566, 845
Prochaska, J. X., Naumov, S. O., Carney, B. W., McWilliam, A., & Wolfe, A. M. 2000, ApJ, 120, 2513
Quinn, P. J., Hernquist, L., & Fullagar, D. P. 1993, ApJ, 403, 74
Raassen, A. J. J., & Uylings, P. H. M. 1998, A&A, 340, 300
The atomic data are available on:
http://www.science.uva.nl/pub/orth/iron/FeII.E1
Reddy, B. E., Tomkin, J., Lambert, D. L., & Allende Prieto, C. 2003, MNRAS, 340, 304
Reshetnikov, V., & Combes, F. 1997, A&A, 324, 80
Reylé, C., & Robin, A. C. 2001, A&A, 373, 886
Robin, A. C., Haywood, M., Créze, M., Ojha, D. K., & Bienaymé, O. 1996, A&A, 305, 125
Salasnich, B., Girardi, L., Weiss, A., & Chiosi, C. 2000, A&A, 361, 1023
Savanov, I. S., Huovelin, J., & Tuominen, I. 1990, A&AS, 86, 531
Simmons, G. J., & Blackwell, D. E. 1982, A&A, 112, 209
Schuster, W. J., & Nissen, P. E. 1989, A&A, 222, 69
Schwarzkopf, U., & Dettmar, R.-J. 2000, A&A, 361, 451

Sikström, C. M., Nilsson, H., Litzén, U., Blom, A., & Lundberg, H. 2002, J. Quant. Spectrosc. Radiat. Transfer, 74, 355
Smith, G., & Raggett, D. St. J. 1981, JPhB, 14, 4015
Sneden, C., Gratton, R. G., & Crocker, D. A. 1991, A&A, 246, 354
Soubiran, C., Bienaymé, O., & Siebert, A. 2003, A&A, 398, 141
Stephens, A. 1999, AJ, 117, 1771
Stephens, A., & Boesgaard, A. M. 2002, AJ, 123, 1647
Takeda, Y. 1995, PASJ, 47, 337
Tautvaišienė, G., Edvardsson, B., Tuominen, I., & Ilyin, I. 2001, A&A, 380, 579
Thévenin, F., & Idiart, T. P. 1999, ApJ, 521, 753
Thielemann, K.-K., Argast, D., Brachwitz, et al. 2002, ApSS, 281, 25
Velázquez, H., & White, S. D. M. 1999, MNRAS, 304, 254
Walker, I. R., Mihos, C., & Hernquist, L. 1996, ApJ, 460, 121
Wickliffe, M. E., & Lawler, J. E. 1997, ApJS, 110, 163
Woosley, S. E., & Weaver, T. A. 1995, ApJS, 101, 181